


---

This is the **accepted version** of the journal article:

Muñoz Enano, Jonathan; Vélez Rasero, Paris; Su, Lijuan; [et al.]. «On the Sensitivity of Reflective-Mode Phase-Variation Sensors Based on Open-Ended Stepped-Impedance Transmission Lines: Theoretical Analysis and Experimental Validation». *IEEE transactions on microwave theory and techniques*, Vol. 69, Issue 1 (January 2021), p. 308-324. DOI 10.1109/TMTT.2020.3023728

---

This version is available at <https://ddd.uab.cat/record/258243>

under the terms of the  **CC BY** COPYRIGHT license

# On the Sensitivity of Reflective-Mode Phase-Variation Sensors Based on Open-Ended Stepped-Impedance Transmission Lines: Theoretical Analysis and Experimental Validation

Jonathan Muñoz-Enano, *Student Member IEEE*, Paris Vélez, *Member IEEE*, Lijuan Su, *Member IEEE*, Marta Gil, Pau Casacuberta, and Ferran Martín, *Fellow IEEE*

**Abstract**— This paper presents an exhaustive study of the sensitivity in reflective-mode phase-variation sensors based on an open-ended transmission line with a step-impedance discontinuity. Such discontinuity delimits the sensing region (which extends up to the open end of the so-called sensing line), from the transmission line section connected to the input port (design line), which is used to enhance the sensitivity. The theoretical analysis provides the design guidelines to achieve a sensor with high sensitivity, as compared to the one based on an ordinary (uniform) line with similar length. In particular, it is shown that for sensitivity optimization, the electrical length of the design line must be set to  $90^\circ$  (or an odd multiple), whereas either a  $90^\circ$  (or an odd multiple) or a  $180^\circ$  (or an even or odd multiple) sensing line can be alternatively used in order to maximize the sensitivity. It is shown that the impedance contrast, defined as the ratio between the characteristic impedances of the design and sensing line, is a key parameter for sensitivity enhancement, and it must be as low or as high as possible for the  $90^\circ$  or  $180^\circ$  sensing lines, respectively. For validation purposes, two prototype devices (one with a  $90^\circ$  and the other one with a  $180^\circ$  sensing line) have been designed and fabricated following the design guidelines. Such devices have been tested by loading the sensing region with several materials with different dielectric constants. As compared to the ordinary line based sensors, it is found that the maximum sensitivity is enhanced by a factor of 19.7 and 11.4 in the phase-variation sensor based on a  $90^\circ$  and  $180^\circ$  sensing line, respectively. Finally, the sensor concept is generalized to a multi-section stepped-impedance transmission line as a means of further increasing the sensitivity, and a prototype device exhibiting 528.7° maximum sensitivity is implemented.

**Index Terms**—Reflective-mode sensor, microwave sensor, phase-variation sensor, microstrip, stepped-impedance transmission line.

## I. INTRODUCTION

PLANAR microwave sensors have attracted the interest of many researchers in recent years. Their low cost and low profile (including the possibility to implement conformal sensors on flexible substrates), their compatibility with fully planar fabrication processes, and with other sensing technologies (e.g., microfluidics, lab-on-a-chip, etc.), their potential for wireless connectivity, and their robustness against hostile and harsh conditions, among others, are key aspects that explain the increasing interest of these sensors

within the microwave community. Other advantageous aspects concern the inherently low cost of microwave generation and detection systems. Moreover, microwave sensors are especially suited for material characterization, since microwaves are very sensitive to the properties of the materials to which they interact (including interaction at different scales, i.e., through the near-field or the far-field).

Probably most planar microwave sensors reported to date are based on frequency variation [1]-[9]. In such sensors, the working principle is typically the variation of the resonance frequency and quality factor of a resonator-loaded line, caused by the presence of the material under test (MUT). These sensors are relatively simple, but a wideband interrogation signal is needed for measurement. Wideband signals are also required in frequency splitting sensors [10]-[16], a variant of frequency variation sensors. Although frequency splitting sensors are not truly differential-mode sensors [17]-[28], their working principle is based on symmetry disruption between the so-called reference (REF) material and the MUT (such materials should be placed on top of two identical resonators symmetrically loading a line) [29].

Although frequency variation and frequency splitting sensors exhibiting good performance have been reported, the main limitation of these sensors concerns the fact that the bandwidth required for measurement is given by the output dynamic range. Thus, implementing sensors with a high dynamic range is possible at the expense of a higher cost of the associated electronics (based on wideband voltage controlled oscillators –VCOs).

According to the previous paragraph, it is clear that the implementation of sensors operating at a single frequency represents a very interesting solution in terms of sensor costs in a real scenario. Examples of single-frequency sensors can be found in the literature, including coupling modulation sensors [30]-[40], differential mode sensors [17],[25],[28] and phase-variation sensors [20],[25]. In this paper, we are interested in reflective-mode phase-variation sensors, due to their simplicity (the structure is a simple one-port network) and low cost (other reflective mode sensors have been recently reported [22],[41],[42]). The specific sensor

---

This work was supported by MINECO-Spain (project TEC2016-75650-R), by Generalitat de Catalunya (project 2017SGR-1159), by Institució Catalana de Recerca i Estudis Avançats (who awarded Ferran Martín), and by FEDER funds. J. Muñoz-Enano acknowledges *Secretaria d'Universitats i Recerca* (Gen. Cat.) and *European Social Fund* for the FI grant. Paris Vélez acknowledges the *Juan de la Cierva* Program for supporting him through Project IJCI-2017-31339. M. Gil acknowledges the

*Universidad Politécnica de Madrid* Young Researchers Support Program (VJIDOCUPM18MGB) for its support.

J. Muñoz-Enano, P. Vélez, L. Su, P. Casacuberta, and F. Martín are with GEMMA/CIMITEC, Departament d'Enginyeria Electrònica, Universitat Autònoma de Barcelona, 08193 Bellaterra, Spain. E-mail: [Ferran.Martin@uab.es](mailto:Ferran.Martin@uab.es).

M. Gil is with Departamento Ingeniería Audiovisual y Comunicaciones, Universidad Politécnica de Madrid, 28031 Madrid, Spain.

structure is an open-ended line with a step-impedance discontinuity, and the main objective of the paper is to carry out an exhaustive sensitivity analysis in order to obtain the design guidelines for sensitivity optimization. Moreover, it is also an objective of the paper to experimentally validate the main conclusions of the analysis. For that purpose, a pair of prototype device sensors are designed, fabricated, and tested (by considering materials with different dielectric constant). To gain insight on the potential of the approach for sensitivity enhancement, the proposed sensors are compared with phase-variation sensors based on ordinary (uniform) lines. As it will be shown, the results demonstrate that the sensitivity can substantially be improved by considering a stepped-impedance transmission line adequately designed (i.e., according to the inferred guidelines). Moreover, a procedure to further optimize the sensitivity, by considering a multi-section step-impedance transmission line, is reported.

The work is organized as follows: Section II reports the structure and working principle of the proposed sensor, and justifies the need to include a step-impedance discontinuity for sensitivity enhancement. The sensitivity analysis is carried out in Section III. Such section ends with the required design conditions for sensitivity optimization, derived from the analysis. Section IV is devoted to the experimental validation, and performance comparison with other sensors based on ordinary (uniform) lines. The generalization of the concept to multiple step-impedance discontinuities is considered in Section V, where it is shown that the sensitivity can be enhanced at wish without the need of elongating the sensing line (a relevant property of the proposed sensors). Moreover, a comparison with other sensors where phase variation is the operating principle is carried out in this section. Finally, the main conclusions are highlighted in Section VI.

## II. THE PROPOSED REFLECTIVE-MODE PHASE-VARIATION SENSOR AND WORKING PRINCIPLE

The typical schematic/topology of the proposed reflective-mode phase-variation sensor is depicted in Fig. 1. It is a one-port network consisting of an open-ended transmission line with a step-impedance discontinuity. The sensitive region, indicated by a dashed rectangle in Fig 1, is delimited by the step discontinuity and the open end of the line. For obvious reasons, such line, with characteristic impedance,  $Z_s$ , and electrical length at the design frequency,  $\phi_s$ , is designated as sensing line. The line section comprised between the step-impedance discontinuity and the input port (with characteristic impedance  $Z$  and electrical length  $\phi$ ), fundamental for sensitivity optimization, is identified as design line in this paper.

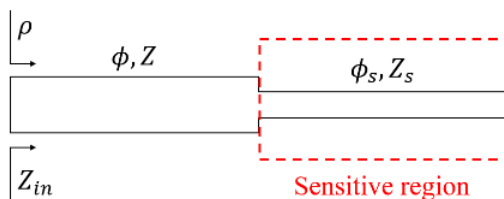


Fig. 1. Typical schematic/topology of the proposed reflective-mode phase-variation sensor based on a step-impedance discontinuity.

This sensor is devoted to material characterization, and the working principle is the variation experienced by the phase of the reflection coefficient,  $\rho$ , when a certain material (material under test –MUT) is placed on top of the sensing region. Note that, ideally (i.e., by excluding the effects of losses), the modulus of the reflection coefficient should be  $|\rho| = 1$ . By considering a uniform and matched open-ended line, i.e., with characteristic impedance identical to the reference impedance of the port,  $Z_0$ , the reflection coefficient is simply [43]

$$\rho = e^{-2j\phi_s} \quad (1)$$

Note that the previous reflection coefficient is the one corresponding to the structure of Fig. 1 by considering  $\phi = 0$  (absence of design line) and  $Z_s = Z_0$ . In such uniform (and matched) line, a variation of the phase of the line,  $\Delta\phi_s$ , produced by a change in the dielectric constant of the MUT, generates a variation in the phase of the reflection coefficient given by

$$\Delta\phi_\rho = -2\Delta\phi_s \quad (2)$$

and, consequently, the sensitivity of the phase of the reflection coefficient,  $\phi_\rho$ , with the phase of the line is simply

$$\frac{d\phi_\rho}{d\phi_s} = -2 \quad (3)$$

However, the key sensor parameter is the sensitivity of  $\phi_\rho$  with the dielectric constant of the MUT,  $\varepsilon_{MUT}$ , given by

$$S = \frac{d\phi_\rho}{d\varepsilon_{MUT}} = \frac{d\phi_\rho}{d\phi_s} \cdot \frac{d\phi_s}{d\varepsilon_{MUT}} \quad (4)$$

In (2)-(4), the effects of  $\varepsilon_{MUT}$  on  $\phi_\rho$  through the variation of  $Z_s$  have been omitted. In general, such effects are not negligible, and should be accounted for by adding an additional term in (4), see Appendix A. However, for the conditions that optimize the sensitivity, to be discussed later, such term is identically null, as demonstrated in Appendix A. Consequently, we adopt expression (4) in the present study, as far as the main objective is the implementation of sensors with optimum sensitivity.

The last derivative on the right-hand side member of (4),  $d\phi_s/d\varepsilon_{MUT}$ , depends on the length of the line, its transverse geometry, and also on the dielectric constant of the substrate,  $\varepsilon_r$ . Obviously, the longer the line, the higher the sensitivity, as it is well known [25], but this strategy for sensitivity enhancement goes against size reduction. The transverse geometry does not have a strong influence on the phase variation, since the effective dielectric constant of the line has a soft dependence on the transverse geometry of the line. Finally, low-dielectric constant substrates favor sensitivity optimization, but there is a limit concerning the sensitivity improvement achievable with this strategy since  $\varepsilon_r > 1$  (moreover, sometimes the substrate is dictated by external constraints or specifications). Thus, in summary, the last derivative in (4) cannot be significantly engineered in order to substantially improve its contribution to the overall sensitivity. Nevertheless, the effects of such term in the total sensitivity will be analyzed at the end of the next section.

Concerning the first term,  $d\phi_\rho/d\phi_s$ , for a uniform and matched line, the value is given by equation (3). However, by introducing further degrees of freedom (i.e., a step-

impedance discontinuity, as depicted in Fig. 1), it is possible to engineer the line and substantially improve the first term on the right-hand side member of (4), as it will be demonstrated in this paper. The design parameters include the characteristic impedances of both the sensing and the design transmission line sections, as well as their electrical lengths. The idea of optimizing the sensitivity in these reflective-mode phase-variation sensors by means of impedance contrast is inspired by the well-known effect of size reduction in half-wavelength or quarter-wavelength stepped-impedance resonators [44], which can be attributed to a further variation of the phase of the signal along the whole element. In particular, stepped-impedance shunt stubs (SISS) with extreme impedance contrast can be considered to be semi-lumped resonators, as discussed in [45].

### III. SENSITIVITY ANALYSIS

The main purpose of this section is to analyze in detail the first term of the right-hand side member of (4),  $d\phi_p/d\phi_s$ , in order to determine the optimum design parameters ( $Z$ ,  $Z_s$ ,  $\phi$  and  $\phi_s$ ) for sensitivity optimization. However, we will also obtain analytically the last derivative in (4), by considering a semi-infinite MUT. This is important since the transverse geometry of the line has influence on this term, but it also determines the characteristic impedance of the sensing line, thereby influencing the first term. Let us first carry out the sensitivity analysis corresponding to the first term of (4),  $d\phi_p/d\phi_s$ , by considering a uniform (not necessarily matched) sensing line directly connected to the input port (i.e., without the presence of the design line, or the discontinuity), and then the general case of the structure with step-impedance discontinuity (Fig. 1). The last subsection will be devoted to the analysis of the last term in (4).

#### A. Sensitivity Analysis for a Uniform and Mismatched Sensing Line Directly Connected to the Input Port

By eliminating the design line (equivalent to consider the general case with  $\phi = 0$ ), the impedance seen from the input port and the reflection coefficient referred to  $Z_0$  (the reference impedance of the port), are given by [43]

$$Z_{in} = -jZ_s \cot \phi_s \quad (5)$$

and

$$\rho = \frac{+Z_0 + jZ_s \cot \phi_s}{-Z_0 + jZ_s \cot \phi_s} \quad (6)$$

respectively. The phase of the reflection coefficient is thus

$$\phi_p = 2\arctan\left(\frac{Z_s \cot \phi_s}{Z_0}\right) \quad (7)$$

and the sensitivity of  $\phi_p$  with  $\phi_s$ , designated as  $S_{\phi_s}$ , is found to be

$$S_{\phi_s} = \frac{d\phi_p}{d\phi_s} = -\frac{2}{\frac{Z_0}{Z_s} \sin^2 \phi_s + \frac{Z_s}{Z_0} \cos^2 \phi_s} \quad (8)$$

Let us now calculate the values of  $\phi_s$  that maximize, or minimize, the sensitivity. For that purpose, the derivative of (8) is calculated. The result can be expressed as

$$\frac{dS_{\phi_s}}{d\phi_s} = \frac{4\left(\frac{Z_0}{Z_s} - \frac{Z_s}{Z_0}\right) \sin \phi_s \cdot \cos \phi_s}{\left(\frac{Z_0}{Z_s} \sin^2 \phi_s + \frac{Z_s}{Z_0} \cos^2 \phi_s\right)^2} \quad (9)$$

For the trivial case with  $Z_s = Z_0$  (matched sensing line), the derivative of the sensitivity is null, as expected since the sensitivity is constant (and given by expression 3). However, if  $Z_s \neq Z_0$ , the values of  $\phi_s$  that provide extreme values to the sensitivity (those that null the numerator of 9) satisfy either  $\phi_s = n\pi$ , or  $\phi_s = (2n + 1)\cdot\pi/2$ , with  $n = 0, 1, 2, \dots$ . The corresponding sensitivities are found to be

$$S_{\phi_s} = -2\frac{Z_0}{Z_s} = -\frac{2}{\overline{Z_s}} \quad \text{for } \phi_s = n\pi \quad (10a)$$

$$S_{\phi_s} = -2\frac{Z_s}{Z_0} = -2\overline{Z_s} \quad \text{for } \phi_s = (2n + 1)\cdot\pi/2 \quad (10b)$$

where  $\overline{Z_s}$  is the normalized impedance of the sensing line. According to expressions (10), for sensitivity optimization, the normalized impedance of the sensing line must be high if the electrical length satisfies  $\phi_s = (2n + 1)\cdot\pi/2$ , and it must be low for  $\phi_s = n\pi$ . Note that the limits are dictated by the maximum and minimum achievable values of the normalized impedance. For instance, if the impedance span is delimited by  $Z_s = 25 \Omega$  (minimum value) and  $Z_s = 150 \Omega$  (maximum value), and  $Z_0 = 50 \Omega$ , the upper limit of the magnitude of the sensitivity is  $|S_{\phi_s, \max}| = 6$  [achieved if  $Z_s = 150 \Omega$ , i.e.,  $\overline{Z_s} = 3$ , and  $\phi_s = (2n + 1)\cdot\pi/2$ ]. Figure 2 depicts a plot of the sensitivity (expression 8) as a function of  $\overline{Z_s}$  and  $\phi_s$ , where the above-cited guidelines for sensitivity optimization are confirmed. It can also be concluded that for  $\overline{Z_s} > 1$ , the sensitivity is maximized and minimized for  $\phi_s = (2n + 1)\cdot\pi/2$  and  $\phi_s = n\pi$ , respectively, whereas for  $\overline{Z_s} < 1$ ,  $\phi_s = n\pi$  provides the maximum value of the sensitivity, and the sensitivity is a minimum for  $\phi_s = (2n + 1)\cdot\pi/2$ .

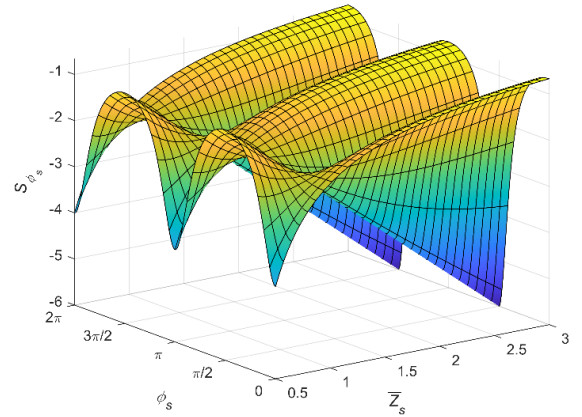


Fig. 2. Plot of the sensitivity of the phase of the reflection coefficient with the phase of the sensing line, for the case of the sensing line directly connected to the input port. Note that the sensitivity takes negative values, but its magnitude is maximized, or minimized, according to the line impedance and electrical length combinations indicated in the text.

#### B. Sensitivity Analysis for an Open-Ended Line with a Step-Impedance Discontinuity (General Case)

In this subsection, the main objective is to explore the possibility of further enhancing the sensitivity by adding degrees of freedom to the phase-variation sensor. For that purpose, the structure of Fig. 1, with a step-impedance discontinuity achieved by cascading a transmission line section between the sensing line and the input port, is considered. In this case, the impedance seen from the input port is

$$Z_{in} = \frac{jZ(Z \tan \phi - Z_s \cot \phi_s)}{Z + Z_s \cot \phi_s \tan \phi} \quad (11)$$

whereas the reflection coefficient is found to be

$$\rho = \frac{-Z_0(Z+Z_s \tan \phi \cot \phi_s) + jZ(Z \tan \phi - Z_s \cot \phi_s)}{+Z_0(Z+Z_s \tan \phi \cot \phi_s) + jZ(Z \tan \phi - Z_s \cot \phi_s)} \quad (12)$$

and the phase of the reflection coefficient is

$$\phi_\rho = 2\arctan\left(\frac{Z(Z_s \cot \phi_s - Z \tan \phi)}{Z_0(Z+Z_s \tan \phi \cot \phi_s)}\right) \quad (13)$$

Let us now evaluate the sensitivity as defined in (8). After some simple calculation, the following result is obtained:

$$S_{\phi_s} = \frac{-2Z^2 Z_s Z_0 (1 + \tan^2 \phi)}{Z_0^2 (Z \sin \phi_s + Z_s \tan \phi \cos \phi_s)^2 + Z^2 (Z \tan \phi \sin \phi_s - Z_s \cos \phi_s)^2} \quad (14)$$

Note that if  $\phi = 0$ , equation (14) simplifies to expression (8), as expected.

Since the main purpose of the analysis is to find the conditions for sensitivity optimization by considering the addition of the design line, it is pertinent to calculate the derivative of  $S_{\phi_s}$  with the electrical length of this line,  $\phi$ . By forcing the resulting expression to be zero, the value of  $\phi$  providing the maximum value of the sensitivity (provided the other design values, i.e.,  $\phi_s$ ,  $Z_s$ , and  $Z$ , are fixed) is expected to be found. However, in order to simplify the calculation, we have inferred the derivative with respect to  $\tan \phi$ . The following result has been found:

$$\frac{dS_{\phi_s}}{d \tan \phi} = -4 \frac{(Z_0^2 Z_A^2 + Z^2 Z_B^2) Z^2 Z_s Z_0 \tan \phi - Z^2 Z_s Z_0 (1 + \tan^2 \phi) (Z_0^2 Z_A Z_s \cos \phi_s + Z^2 Z_B Z \sin \phi_s)}{(Z_0^2 Z_A^2 + Z^2 Z_B^2)^2} \quad (15)$$

where we have used  $Z_A$  and  $Z_B$ , defined as

$$Z_A = Z \sin \phi_s + Z_s \tan \phi \cos \phi_s \quad (16a)$$

$$Z_B = Z \tan \phi \sin \phi_s - Z_s \cos \phi_s \quad (16b)$$

for simplification purposes. The zero (or zeros) in (15) are given by those values of  $\tan \phi$  that null the numerator. Thus, rearranging the numerator and forcing it to be zero, the following second order equation ( $\tan \phi$  being the unknown) results:

$$ZZ_s \sin \phi_s \cos \phi_s \tan^2 \phi + (Z^2 \sin^2 \phi_s - Z_s^2 \cos^2 \phi_s) \tan \phi - ZZ_s \sin \phi_s \cos \phi_s = 0 \quad (17)$$

and the two solutions ( $\phi = \phi_1$  and  $\phi = \phi_2$ ) are

$$\tan \phi_1 = \frac{Z_s \cos \phi_s}{Z \sin \phi_s} \quad (18a)$$

$$\tan \phi_2 = -\frac{Z \sin \phi_s}{Z_s \cos \phi_s} \quad (18b)$$

Thus, for  $\phi_1$  and  $\phi_2$  given by (18), the sensitivity (calculated using 14), should be a local (or absolute) maximum or minimum. The specific values are:

$$S_{\phi_s} \Big|_{\phi_1} = -\frac{2Z^2 Z_s}{Z_0} \frac{1}{Z^2 \sin^2 \phi_s + Z_s^2 \cos^2 \phi_s} \quad (19a)$$

$$S_{\phi_s} \Big|_{\phi_2} = -2Z_0 Z_s \frac{1}{Z^2 \sin^2 \phi_s + Z_s^2 \cos^2 \phi_s} \quad (19b)$$

Nevertheless, in order to be sure that the convenient value of  $\phi$  for sensitivity optimization is either  $\phi_1$  or  $\phi_2$ , it should be verified that  $S_{\phi_s}$  does not exhibit poles (zeros in the denominator). Inspection of (14) reveals that the denominator cannot be zero, unless both squared terms are simultaneously null, and this is not possible.

In view of expressions (19), it follows that if  $Z < Z_0$ , the sensitivity is larger for  $\phi_2$ , and it is larger for  $\phi_1$  if  $Z > Z_0$ . Let us now calculate the derivative of expressions (19) with  $\phi_s$ , in order to calculate the value of  $\phi_s$  that maximizes, or minimizes, these values. The following values are obtained:

$$\frac{dS_{\phi_s} \Big|_{\phi_1}}{d\phi_s} = \frac{4Z^2 Z_s}{Z_0} \frac{(Z^2 - Z_s^2) \sin \phi_s \cos \phi_s}{(Z^2 \sin^2 \phi_s + Z_s^2 \cos^2 \phi_s)^2} \quad (20a)$$

$$\frac{dS_{\phi_s} \Big|_{\phi_2}}{d\phi_s} = 4Z_0 Z_s \frac{(Z^2 - Z_s^2) \sin \phi_s \cos \phi_s}{(Z^2 \sin^2 \phi_s + Z_s^2 \cos^2 \phi_s)^2} \quad (20b)$$

and for both equations, the derivative is null if  $\phi_s = n\pi$ , or  $\phi_s = (2n + 1)\pi/2$ .

Concerning (20a), if  $\phi_s = (2n + 1)\pi/2$ , then  $\phi_1 = n\pi$ , according to (18). Conversely, if  $\phi_s = n\pi$ , then it follows that  $\phi_1 = (2n + 1)\pi/2$ . The sensitivity in the former case is

$$S_{\phi_s} = \frac{-2Z_s}{Z_0} = -2\bar{Z}_s \quad (21)$$

and the following value results for  $\phi_s = n\pi$ , and  $\phi_1 = (2n + 1)\pi/2$ :

$$S_{\phi_s} = \frac{-2Z^2}{Z_0 Z_s} = -2\frac{\bar{Z}^2}{\bar{Z}_s} \quad (22)$$

It is clear in view of (21) and (22) that for  $Z > Z_0 > Z_s$ , (22) is a maximum and (21) is a minimum.

Concerning (20b), if  $\phi_s = (2n + 1)\pi/2$ , then  $\phi_2 = (2n + 1)\pi/2$ , and  $\phi_2 = n\pi$  if  $\phi_s = n\pi$ . The sensitivity in the former case is

$$S_{\phi_s} = \frac{-2Z_0 Z_s}{Z^2} = -2\frac{\bar{Z}_s}{\bar{Z}^2} \quad (23)$$

For  $\phi_2 = n\pi$  and  $\phi_s = n\pi$ , the sensitivity is found to be:

$$S_{\phi_s} = \frac{-2Z_0}{Z_s} = -2\frac{1}{\bar{Z}_s} \quad (24)$$

Inspection of (23) and (24) reveals that for  $Z < Z_0 < Z_s$ , (23) is a maximum and (24) is a minimum.

According to the previous analysis, it can be concluded that for sensitivity optimization, there are two optimum combinations regarding the electrical lengths of the sensing and design lines (plus the corresponding multiples):

- Case A:  $\phi_s = (2n + 1)\pi/2$  and  $\phi = (2n + 1)\pi/2$ . In this case, the line impedances should satisfy  $Z < Z_0 < Z_s$ , and the value of the sensitivity is given by (23), corresponding to a maximum. Moreover, the lower the impedance contrast, defined as the ratio between the characteristic impedances of the design and sensing line, the higher the sensitivity.
- Case B:  $\phi_s = n\pi$  and  $\phi = (2n + 1)\pi/2$ . In this case, the line impedances should satisfy  $Z > Z_0 > Z_s$ , and the value of the sensitivity is given by (22), also corresponding to a maximum. A high impedance contrast enhances the sensitivity, in this case.

It is interesting to compare the values of the maximum sensitivities, given by (22) and (23) for the  $\phi_s = n\pi$  and  $\phi_s = (2n + 1)\pi/2$  sensing lines, respectively, with the corresponding values without design line, given by (10a) and (10b). The ratio for  $\phi_s = (2n + 1)\pi/2$  is  $1/\bar{Z}^2$ , whereas it is  $\bar{Z}^2$  for  $\phi_s = n\pi$ . According to these values, the sensitivity can be substantially enhanced by including the so-called design line with the adequate impedance value (low for  $\phi_s = (2n + 1)\pi/2$ ,

and high for  $\phi_s = n \cdot \pi$ ). The reason is that the dependence of such ratios with the normalized impedance of the design line is squared.

Figure 3 plots the dependence of the sensitivity  $S_{\phi_s}$  with  $\phi_s$  and  $\phi$ , calculated by means of expression (14), for two cases: (i)  $Z < Z_0 < Z_s$ , and (ii)  $Z > Z_0 > Z_s$ . The figure confirms that the sensitivity is optimum (maximum) for the phase combinations predicted by the analysis. It is also interesting to mention that for any value of  $\phi_s$ , there are two values of  $\phi$  in the interval  $[0-\pi]$  (designated as  $\phi_1$  and  $\phi_2$  in expression 18), where the sensitivity is either a maximum or a minimum. The positions of the maxima in the  $\phi$ - $\phi_s$  plane are indicated in Fig. 3 (blue regions). Note that these positions converge to the canonical values if the electrical length of the sensing line is either  $\phi_s = n \cdot \pi$  or  $\phi_s = (2n + 1) \cdot \pi/2$ .

The maximum value of the magnitude of the sensitivity for the two cases considered in Fig. 3, given by equation (22) for  $Z = 150 \Omega$  and  $Z_s = 25 \Omega$ , and by equation (23) for  $Z = 25 \Omega$  and  $Z_s = 150 \Omega$ , are found to be  $|S_{\phi_s}| = 36$  and  $|S_{\phi_s}| = 24$ , respectively. With these high values of the sensitivity of the phase of the reflection coefficient with the phase of the sensing line, it is expected that the overall sensitivity, given by expression (4), can be significantly optimized. Interestingly, these high sensitivity values have been achieved with perfectly implementable transmission lines (i.e., the considered high,  $150 \Omega$ , and low,  $25 \Omega$ , characteristic impedances correspond to implementable line widths, at least in microstrip technology and line implementation in most commercial microwave substrates).

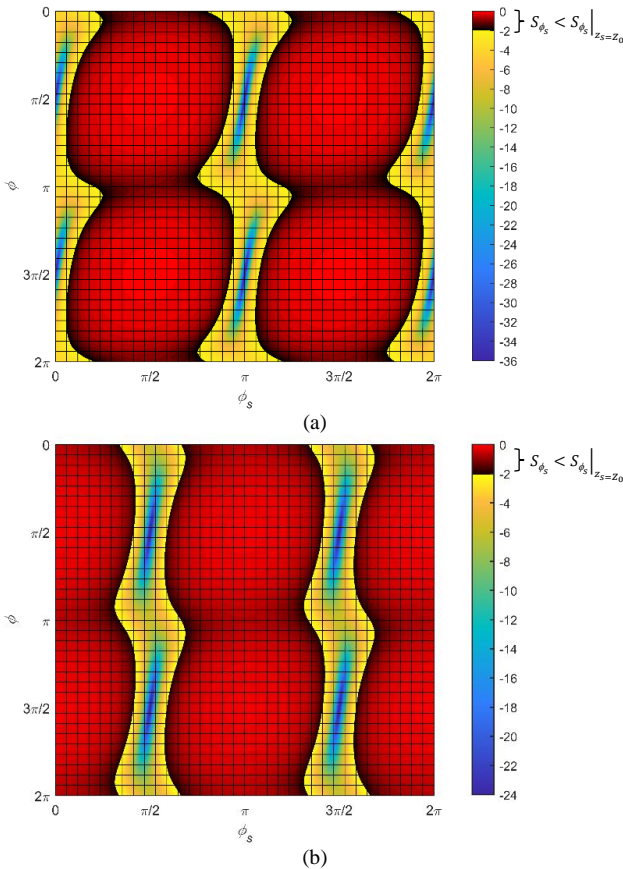


Fig. 3. Plot of the sensitivity of the phase of the reflection coefficient with the phase of the sensing line, as a function of the electrical lengths of the sensing and design lines, for two cases: (a)  $Z = 150 \Omega$  and  $Z_s = 25 \Omega$ ; (b)  $Z = 25 \Omega$  and  $Z_s = 150 \Omega$ . The reference impedance of the port is  $Z_0 = 50 \Omega$ . In this case, the sensitivity is presented in level charts, rather than three-dimensional views, for better comprehension.

### C. Sensitivity of the Phase of the Sensing Line with the Dielectric Constant of the MUT

For the calculation of the last derivative in (4),  $d\phi_s/d\varepsilon_{MUT}$ , let us first express the phase of the sensing line in terms of the effective dielectric constant of the line,  $\varepsilon_{eff}$ , i.e.,

$$\phi_s = \frac{\omega l_s}{c} \sqrt{\varepsilon_{eff}} \quad (25)$$

In (25),  $l_s$  is the length of the sensing line,  $\omega$  is the angular frequency, and  $c$  is the speed of light in vacuum. By considering a semi-infinite MUT (in the vertical direction) on top of the sensing line, the effective dielectric constant can be expressed as [43]

$$\varepsilon_{eff} = \frac{\varepsilon_r + \varepsilon_{MUT}}{2} + \frac{\varepsilon_r - \varepsilon_{MUT}}{2} F \quad (26)$$

where  $\varepsilon_r$  is the dielectric constant of the substrate and  $F$  is a geometry factor given by

$$F = \left(1 + 12 \frac{h}{W_s}\right)^{-1/2} \quad (27a)$$

for  $W_s/h \geq 1$ , or by

$$F = \left(1 + 12 \frac{h}{W_s}\right)^{-1/2} + 0.04 \left(1 - \frac{W_s}{h}\right)^2 \quad (27b)$$

for  $W_s/h < 1$ . In (27),  $h$  and  $W_s$  are the substrate thickness and the width of the sensing line, respectively, and it is assumed that  $t \ll h$ , where  $t$  is the thickness of the metallic layer. In practice, if the MUT is thick enough, so that the electromagnetic field generated by the line does not reach the MUT-air interface, the MUT can be considered to be semi-infinite, and equation (26) can be used for analysis purposes.

The last term in (4) can be expressed as

$$\frac{d\phi_s}{d\varepsilon_{MUT}} = \frac{d\phi_s}{d\varepsilon_{eff}} \frac{d\varepsilon_{eff}}{d\varepsilon_{MUT}} = \frac{\omega l_s}{4c \sqrt{\varepsilon_{eff}}} (1 - F) \quad (28)$$

and introducing (26) in (28), after some simple algebra one obtains

$$\frac{d\phi_s}{d\varepsilon_{MUT}} = \frac{\omega l_s}{2\sqrt{2}c} \frac{1}{\sqrt{\varepsilon_r \frac{1+F}{(1-F)^2} + \varepsilon_{MUT} \frac{1}{1-F}}} \quad (29)$$

It is apparent by inspection of (29) that operating at high frequency and/or choosing a long sensing line favors sensitivity (as it was anticipated before, and it is well known). For sensitivity optimization, it is also convenient to select the substrate with the smallest possible dielectric constant. The effects of the transverse geometry of the line are included in  $F$ . From (27), it follows that  $F$  decreases by increasing  $h$  or by decreasing  $W_s$ . A decrease in  $F$  favors the sensitivity, as it can be easily deduced from (29). Therefore, for sensitivity optimization it is convenient to deal with high impedance sensing lines, as far as for the implementation of these lines, either narrow line widths and/or or thick substrates are needed. According to these comments, the preferred option for the implementation of the sensors is to choose the line impedances satisfying  $Z < Z_0 < Z_s$ , rather than  $Z > Z_0 > Z_s$ . However, the final decision should be taken by considering the maximum and minimum achievable line impedances (determined by the substrate in use and by the available fabrication technology), and evaluating the whole sensitivity using (4), (29), and either (22) or (23) depending on each case.

It should also be mentioned that if the thickness of the MUT does not obey the semi-infinite requirement criterion,

expression (29) cannot be considered to be valid, and thereby it cannot be used to predict the overall sensitivity of the sensor. Nevertheless, the conclusions of the previous paragraph, on the effects of the substrate characteristics (dielectric constant) and transverse geometry of the line on sensitivity, do hold.

#### IV. EXPERIMENTAL VALIDATION

Experimental validation of the theory of the preceding section is carried out by considering two prototype sensors based on a step-impedance discontinuity. In one case, the line impedances and electrical lengths satisfy  $Z < Z_0 < Z_s$ ,  $\phi_s = (2n + 1) \cdot \pi/2$  and  $\phi = (2n + 1) \cdot \pi/2$  (case A of the previous Section). For the second prototype, the transmission line sections are chosen following the guidelines corresponding to case B of Section III, i.e.,  $Z > Z_0 > Z_s$ ,  $\phi_s = n \cdot \pi$  and  $\phi = (2n + 1) \cdot \pi/2$ . Moreover, for comparison purposes, a set of four sensors without the presence of the design line (i.e., without step-impedance discontinuity), and lengths comparable to those of the step-impedance discontinuity based sensors, are also designed and fabricated. All sensors are fabricated on the *Rogers RO4003C* substrate with dielectric constant  $\epsilon_r = 3.55$ , thickness  $h = 1.524$  mm and loss factor  $\tan\delta = 0.0022$  (the prototypes are fabricated by means of the *LPKF H100* drilling machine), and the frequency of operation is set to  $f = 2$  GHz.

For case A, the line impedances are set to  $Z = 25\Omega$  and  $Z_s = 150\Omega$  (with  $Z_0 = 50\Omega$ ). With these values, the width of the lines, inferred from the transmission line calculator included in *Keysight ADS*, have been found to be  $W_s = 0.242$  mm and  $W = 9.1$  mm, where  $W$  is the width of the design line. The electrical lengths of both the design and sensing line are set to  $\phi = \phi_s = 90^\circ$ , in order to implement the sensor with the minimum physical length. Note that the sensitivity can be improved by elongating the sensing line (considering an electrical length equal to an odd multiple of  $90^\circ$ ). However, the objective in this paper is to demonstrate the potential for sensitivity improvement with the proposed strategy (step-impedance discontinuity), leading to high sensitivity phase-variation sensors compatible with small sizes. The calculated physical lengths of the design and sensing lines are  $l = 18.3$  mm and  $l_s = 23.65$  mm, respectively (note that these lengths are unequal since the phase velocities of the design and sensing lines are not identical). The photograph of the designed sensor is depicted in Fig. 4(a), where it can be appreciated that a  $50\text{-}\Omega$  access line (with length of 10 mm) has been added for connector soldering (the width of this  $50\text{-}\Omega$  line is 3.42 mm).

The second sensor (case B) has been designed with the following values of characteristic impedances and electrical lengths:  $Z = 150\Omega$ ,  $Z_s = 25\Omega$ ,  $\phi = 90^\circ$ , and  $\phi_s = 180^\circ$ . Line widths and lengths are in this case  $W = 0.242$  mm,  $W_s = 9.1$  mm,  $l = 20.7$  mm and  $l_s = 42.1$  mm. The photograph of this prototype sensor is shown in Fig. 4(b).

Finally, an additional set of four sensors, based on uniform lines, has been designed according to the following considerations. One sensor is implemented by means of a  $\phi_s = 90^\circ$  sensing line with high characteristic impedance ( $Z_s = 150\Omega$ ), in order to achieve good sensitivity [see 10(b)]. Another sensor consists of a low-impedance ( $Z_s = 25\Omega$ ) sensing line with electrical length  $\phi_s = 180^\circ$  [according to the

high sensitivity criterion of 10(a)]. Finally, the last two sensors are simply a  $180^\circ$  and  $90^\circ$  uniform and matched ( $50\text{-}\Omega$ ) lines. These four sensors are also depicted in Fig. 4, where the inclusion of the  $50\text{-}\Omega$  access lines can be appreciated. The lengths of these access lines have been chosen in order to achieve sensors with comparable lengths, i.e., for those with identical sensing lines. The sensing regions are indicated by the dashed rectangles.

For the six fabricated sensors, we have placed on top of the sensing areas several dielectric slabs with different dielectric constants. Such slabs are uncoated microwave substrates with well-known dielectric constant. Their thickness is roughly 3 mm (achieved by stacking up two 1.5-mm slabs). With this thickness, the MUT can be considered to be semi-infinite in the vertical direction, as it has been inferred from independent simulations (not shown), indicating that the phase of the reflection coefficient does not significantly vary for thicker MUT slabs. Figure 5 depicts the variation of the phase of the reflection coefficient experienced by the different sensors for the different dielectric loads (indicated in the caption of Fig. 5). The measurement of the reflection coefficient has been inferred by means of the *Keysight 85072A* vector network analyzer. It can be seen that the sensors with step-impedance discontinuity exhibit stronger variation of the phase of the reflection coefficient with the dielectric constant of the material under test. By contrast, sensors of Fig. 4(e) and Fig. 4(f), based on a uniform matched line, exhibit the softer dependence. Thus, these results point out the potential of step-impedance lines for sensitivity enhancement, provided the electrical length and characteristic impedance of the line sections is adequately selected.

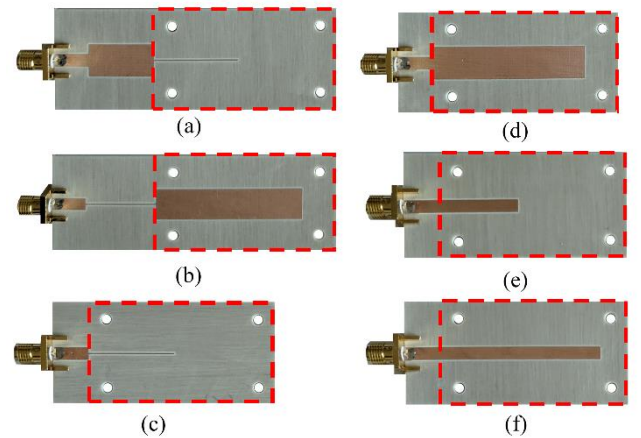


Fig. 4. Photographs of the fabricated reflective-mode phase-variation sensors. (a) Sensor with step-impedance discontinuity and  $Z < Z_0 < Z_s$ ; (b) sensor with step-impedance discontinuity and  $Z > Z_0 > Z_s$ ; (c) sensor with uniform mismatched sensing line and  $Z_s > Z_0$ ; (d) sensor with uniform mismatched sensing line and  $Z_s < Z_0$ ; (e) sensor based on a  $90^\circ$  uniform  $50\text{-}\Omega$  sensing line and (f) sensor based on a  $180^\circ$  uniform  $50\text{-}\Omega$  sensing line.

Figure 5 also includes the simulation results, inferred by means of the *Ansys HFSS* commercial software. The agreement with the measured data is very good. In order to validate the sensitivity analysis carried out in Section III, we have included further simulated data points by considering additional hypothetical materials with different dielectric constants in the range between  $\epsilon_{MUT} = 1$  to  $\epsilon_{MUT} = 10.5$ . From the simulated data points, we have obtained the sensitivity, also included in Fig. 5. The sensitivity in the limit when

$\Delta \varepsilon_{MUT} = \varepsilon_{MUT} - \varepsilon_{REF} \rightarrow 0$  ( $\varepsilon_{REF}$  being the dielectric constant of vacuum, i.e.,  $\varepsilon_{REF} = 1$ ) is indicated in Fig. 5 for each sensor. We have calculated the sensitivity for  $\varepsilon_{MUT} = 1$  by means of expression (4), where the last term is given by (29), and the first term ( $S_{\phi}$ ) is obtained by means of (3), (10a), (10b), (22) or (23), depending on the specific sensor. These theoretical sensitivities, designated as  $S_{th}$ , are also indicated in Fig. 5. As it can be seen, the agreement with the sensitivities inferred from the simulated data points,  $S$ , is very good, thereby validating the sensitivity analysis developed in the preceding section.

It is remarkable that the sensitivity for small perturbations is significantly enhanced by considering the step-impedance discontinuity. Note that for the sensor of Fig. 4(a), the sensitivity is roughly 4 times larger than the one of the sensor of Fig. 4(c), with identical sensing line, and 19.7 times larger than the one of the sensor of Fig. 4(e). On the other hand, the sensor of Fig. 4(b) exhibits a sensitivity better than the one of the sensors of Figs. 4(d) and 4(f) by a factor of 9 and 11.4, respectively.

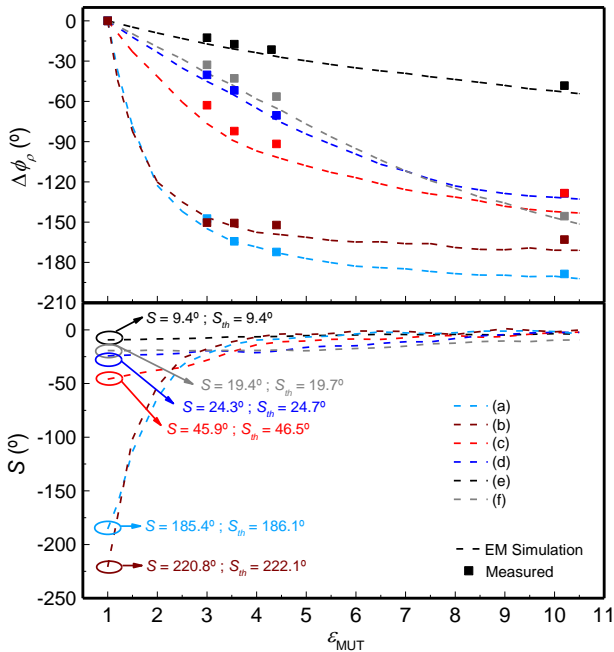


Fig. 5. Measured and simulated phase of the reflection coefficient for the sensors of Fig. 4, and simulated sensitivity. (a) Sensor with step-impedance discontinuity and  $Z < Z_0 < Z_s$ ; (b) sensor with step-impedance discontinuity and  $Z > Z_0 > Z_s$ ; (c) sensor with uniform mismatched sensing line and  $Z_s > Z_0$ ; (d) sensor with uniform mismatched sensing line and  $Z_s < Z_0$ ; (e) sensor based on a  $90^\circ$  uniform  $50\text{-}\Omega$  sensing line and (f), sensor based on a  $180^\circ$  uniform  $50\text{-}\Omega$  sensing line. The measured dielectric loads are 3-mm slabs of uncoated PLA ( $\varepsilon_{MUT} = 3$ ), Rogers RO4003C ( $\varepsilon_{MUT} = 3.55$ ), FR4 ( $\varepsilon_{MUT} = 4.4$ ) and Rogers RO3010 ( $\varepsilon_{MUT} = 10.2$ ) substrates. The sensitivities in the limit of small perturbations are given in absolute value.

It can be seen in Fig. 5 that as  $\varepsilon_{MUT}$  increases, the magnitude of the sensitivity decreases, and such decrement is more pronounced for the sensors exhibiting the larger sensitivity for small perturbations, i.e., those including the step-impedance discontinuity. These sensors exhibit smaller linearity, as compared to those based on uniform matched lines, but they are able to detect tiny variations of the dielectric constant as compared to the one of a reference material by virtue of their high sensitivity. Since the sensing lines have been designed in order to exhibit either  $90^\circ$  or  $180^\circ$  by considering that they are unloaded, it follows that the reference dielectric constant in our study is the one of air, and

for this reason the sensitive is a maximum for  $\varepsilon_{MUT} = 1$ . Nevertheless, highly sensitive dielectric constant measurements in the vicinity of a different reference value are possible by simply forcing the sensing lines to exhibit the required electrical length ( $90^\circ$  or  $180^\circ$ ) at the operating frequency and the required value of  $Z_s$  when they are loaded with the reference sample. For instance, by considering the Rogers RO4003C with dielectric constant 3.55 as reference sample, it is expected that the phase of the reflection coefficient for the different considered MUT can be clearly distinguished (nevertheless, further designs and validations are out of the scope of this paper).

## V. GENERALIZATION OF THE CONCEPT AND DISCUSSION

It has been theoretically demonstrated and experimentally validated in this paper that a step-impedance discontinuity is useful to increase the sensitivity in these reflective-mode phase-variation sensors. Moreover, it has been shown that the electrical length of the design line must be set to  $\phi = (2n + 1) \cdot \pi/2$ , whereas either a  $\phi_s = (2n + 1) \cdot \pi/2$  or a  $\phi_s = n \cdot \pi$  sensing line is needed for that purpose (in each case, with the convenient impedance contrast, as discussed in Section III). In this section, it is shown that the sensitivity of the phase of the reflection coefficient with the phase of the sensing line (and thereby the overall sensitivity) for small perturbations can be further improved by considering a multi-step-impedance transmission line, as the one shown in Fig. 6(a). It is a generalization of the structure of Fig. 1, based on a cascade of high and low impedance transmission line sections of identical electrical length, i.e.,  $\phi = (2n + 1) \cdot \pi/2$ , followed by the sensing line (with electrical length  $\phi_s$  and characteristic impedance  $Z_s$ ). The characteristic impedances of the high or low impedance transmission line sections are designated by  $Z_i$ , where  $i = 1, 2, \dots, N$  denotes the specific section, and  $N$  is the total number of Sections (e.g.,  $N = 1$  for the structure of Fig. 1).

According to Fig. 6, the impedance seen from the discontinuity in contact with the sensing line, looking at the open end, is called  $Z_{in,s}$ , and it is given by expression (5). The impedance seen from any other discontinuity looking at the open end of the structure,  $Z_{in,i}$ , can be expressed in terms of the impedance seen from the previous discontinuity as

$$Z_{in,i} = \frac{Z_i^2}{Z_{in,i-1}} \quad (30)$$

from which it follows (using mathematical induction) that the impedance seen from the input port can be expressed as

$$Z_{in,N} = Z_{in,s}^{(-1)^N} \cdot \prod_{i=1}^N \{Z_i^{2 \cdot (-1)^{i+N}}\} \quad (31)$$

or (using 5)

$$Z_{in,N} = (-jZ_s)^{(-1)^N} \cdot (\cot \phi_s)^{(-1)^N} \cdot \prod_{i=1}^N \{Z_i^{2 \cdot (-1)^{i+N}}\} \quad (32)$$

In (31) and (32), the symbol  $\Pi$  denotes the product operator.

The reflection coefficient seen from the input port is thus

$$\rho = \frac{j^{(-1)^{N+1}} \cdot (Z_s \cot \phi_s)^{(-1)^N} \cdot \Pi - Z_0}{j^{(-1)^{N+1}} \cdot (Z_s \cot \phi_s)^{(-1)^N} \cdot \Pi + Z_0} \quad (33)$$

and the phase of the reflection coefficient is given by



$$\phi_\rho = 2\arctan\left(\frac{(-1)^N (Z_s \cot \phi_s)^{(-1)^N} \cdot \Pi}{Z_0}\right) \quad (34)$$

Note that in (33) and (34) the argument of the product operator has been omitted for simplicity. After some simple (but tedious) algebra, the sensitivity of  $\phi_\rho$  with  $\phi_s$ , designated as  $S_{\phi_s}$  in (8), is found to be

$$S_{\phi_s} = -\frac{2}{\frac{Z_0}{\Pi \cdot (Z_s)^{(-1)^N}} \frac{(\sin \phi_s)^{(-1)^{N+1}}}{(\cos \phi_s)^{(-1)^{N-1}}} + \frac{\Pi \cdot (Z_s)^{(-1)^N}}{Z_0} \frac{(\cos \phi_s)^{(-1)^{N+1}}}{(\sin \phi_s)^{(-1)^{N-1}}}} \quad (35)$$

and it takes a maximum, or a minimum, value, depending on the set of impedances  $Z_i$ , when the electrical length of the sensing line is either  $\phi_s = (2n + 1) \cdot \pi/2$  or  $\phi_s = n \cdot \pi$ , as anticipated before. In order to evaluate (35) for these specific values of  $\phi_s$ , it is necessary to distinguish if the number of sections,  $N$ , is even or odd. Consequently, four different cases appear, and, for each case, the sensitivity is found to be:

- Case A':  $\phi_s = (2n + 1) \cdot \pi/2$  and  $N$  odd.

$$S_{\phi_s} = -\frac{2Z_s Z_0}{\prod_{i=1}^N \{Z_i^{2 \cdot (-1)^{i+N}}\}} \quad (36a)$$

- Case B':  $\phi_s = n \cdot \pi$  and  $N$  odd.

$$S_{\phi_s} = -\frac{2 \cdot \prod_{i=1}^N \{Z_i^{2 \cdot (-1)^{i+N}}\}}{Z_s Z_0} \quad (36b)$$

- Case C':  $\phi_s = (2n + 1) \cdot \pi/2$  and  $N$  even.

$$S_{\phi_s} = -\frac{2Z_s \cdot \prod_{i=1}^N \{Z_i^{2 \cdot (-1)^{i+N}}\}}{Z_0} \quad (36c)$$

- Case D':  $\phi_s = n \cdot \pi$  and  $N$  even.

$$S_{\phi_s} = -\frac{2Z_0}{Z_s \cdot \prod_{i=1}^N \{Z_i^{2 \cdot (-1)^{i+N}}\}} \quad (36d)$$

Note that for  $N = 1$  (cases A' and B'), expressions (36a) and (36b) coincide with expressions (23) and (22), respectively, as expected, since the multi-stepped impedance transmission line for this case is the one of Fig. 1.

Inspection of expressions (36) reveals that  $Z_s$  appears in the numerator for  $\phi_s = (2n + 1) \cdot \pi/2$  and it appears in the denominator for  $\phi_s = n \cdot \pi$ . Thus, it can be concluded that for quarter-wavelength (or odd multiple) sensing lines, a high characteristic impedance is required for sensitivity optimization (regardless of the number of sections of the structure). Conversely, low impedance values are needed in half-wavelength (or multiple) sensing lines. To infer the effects of the characteristic impedances of the quarter-wavelength transmission line sections,  $Z_i$  (with  $i = 1, 2, \dots, N$ ), on the sensitivity, we should analyze carefully the product operator that appears in expressions (36). For  $N$  odd (cases A' and B'), it follows that the characteristic impedance of a section with odd order (i.e., with  $i$  odd) appears as  $Z_i^2$ , whereas for an even-order section the corresponding term in the product is  $Z_i^{-2}$ . Under these circumstances, the requirement of a high or low value of  $Z_i$  for sensitivity optimization depends on whether the product operator is present either in the numerator or in the denominator in

expressions (36). Particularly, for case A', with the product operator in the denominator, the odd-order transmission line sections must exhibit low impedance values, whereas high characteristic impedance sections are required for the even sections. The opposite conditions apply for case B', as far as the product operator appears in the numerator of (36b). For  $N$  even (cases C' and D') and  $i$  odd, the impedance is negative squared ( $Z_i^{-2}$ ), whereas it appears as  $Z_i^2$  for  $N$  even and  $i$  even. Consequently, for case C', with the product operator in the numerator of (36c), the odd sections must exhibit low characteristic impedance, and the line impedance must be high for the even sections. Finally, it is obvious that for case D' (half-wavelength sensing line), the sections that should exhibit high impedance for sensitivity optimization are those with odd index.

From the previous analysis, it can be concluded that for sensitivity optimization, regardless of the number of sections  $N$ , if the electrical length of the sensing line is  $\phi_s = (2n + 1) \cdot \pi/2$ , the impedance of this line must be high, and the impedance of the cascaded quarter-wavelength sections must alternatively exhibit low and high values (with a low impedance value for the section adjacent to the sensing line, i.e., the one with  $i = 1$ ). For  $\phi_s = n \cdot \pi$ , the sensing line must be a low-impedance line, a high-impedance line is required for the first section ( $i = 1$ ), a low-impedance line for the second section, and so on. Thus, it is clear that a non-uniform stepped-impedance transmission line based on quarter wavelength sections, cascaded to an open-ended quarter- or half-wavelength line, is a very useful structure for sensitivity enhancement in phase-variation sensors. Note that, with the reported approach, the sensitivity can be as high as desired, without the need to increase the length of the sensing line (as occurs in typical phase-variation sensors [20],[25]). For that purpose, it suffices to include the necessary number of sections (with as much contrast of impedance as possible) to obtain the required (high or low) value of the product operator in (36).

Note that the effects of losses on sensor performance (sensitivity) have not been considered so far. From the analysis developed in detail in Appendix B, it can be concluded that the sensitivity is not substantially degraded, at least under the low-loss approximation (an approximation valid for many MUTs). It should also be clarified that although in the Appendix B a method for estimating the loss tangent of the MUT is suggested (see last part), resonant methods are, in general, preferred for that purpose. In the present study, validation of the theoretical analysis is carried out by considering samples with different dielectric constants, and also with different loss tangents. Nevertheless, the considered input variable is the dielectric constant of the MUT. Note, however, that the proposed phase-variation sensors can be applied to material analysis and composition, quality control processes, or to defect detection in samples, since changes in the dielectric constant of the MUT are involved in these applications. Through a proper design, the proposed sensing strategy may be also useful for the characterization of liquid composition (e.g., determination of solute content in liquid solutions, etc.). Nevertheless, this is out of the scope of the present paper.

Despite the fact that the reported experimental results of Section IV (with  $N = 1$ ) are indicative of the potential of the

approach for sensitivity enhancement, let us consider a further example, corresponding to case C' with  $N = 2$ . The impedances are set to  $Z_s = 150 \Omega$ ,  $Z_1 = 25 \Omega$  and  $Z_2 = 86.6 \Omega$  (the operating frequency and substrate characteristics are identical to those of the prototypes of Section IV). The impedance  $Z_2$  has been chosen in order to obtain  $S_{\phi_s} = 72$ , i.e., 3 times the sensitivity of the previous structure with  $Z_s = 150 \Omega$  and  $Z = 25 \Omega$  ( $N = 1$ ). Figure 6(b) shows the photograph of the fabricated prototype.

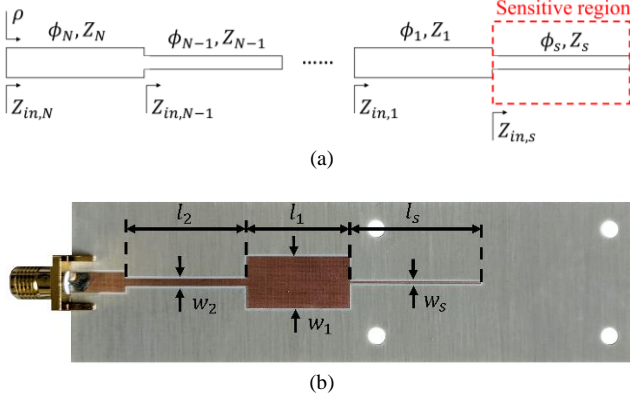


Fig. 6. General schematic/topology of the  $N$ -sections reflective-mode phase-variation sensor (a) and photograph of the fabricated device with  $N = 2$  (b). Dimensions (in mm) are  $w_s = 0.242$ ,  $l_s = 23.65$ ,  $w_1 = 9.1$ ,  $l_1 = 18.3$ ,  $w_2 = 1.22$  and  $l_2 = 21.5$ .

The phase variations of the reflection coefficient, in reference to the one of the bare sensor, inferred from full wave electromagnetic simulation by considering MUTs with dielectric constants varying in the interval 1 to 4, are depicted in Fig. 7. From these simulated data, the sensitivity in the low-perturbation limit ( $\epsilon_{MUT} \approx 1$ ) is found to be  $|S| = 528.7^\circ$ , by far superior to those achieved in the structures with  $N = 1$  of Section IV. As indicated before, with the considered impedance values, the sensitivity of the phase of the reflection coefficient with the phase of the sensing line (calculated from 36c) is found to be  $S_{\phi_s} = -72$ . The sensitivity of  $\phi_s$  with  $\epsilon_{MUT}$  was calculated in the previous section (i.e.,  $d\phi_s/d\epsilon_{MUT} = 7.75^\circ$ ), since in one of the prototypes of that section the sensing line is identical to the one considered in the sensor of Fig. 6. From the product (see 4), the total sensitivity is found to be  $|S_{th}| = 558^\circ$ , in reasonable agreement with the result inferred from full wave simulation. The discrepancy is mainly attributed to the excessive variation of  $\Delta\phi_\rho$  with  $\epsilon_{MUT}$ , which limits the accurate calculation of the sensitivity from the derivative of a set of discrete data points. Nevertheless, potential non-ideality effects caused by the step discontinuities, not considered in the theoretical analysis, may play also a role.

Due to the lack of available samples with  $\epsilon_{MUT}$  in the high sensitive region ( $\epsilon_{MUT} \approx 1$ ), we have carried out an experiment consisting of obtaining the phase of the reflection coefficient for a MUT with dielectric constant  $\epsilon_{MUT} = 3.55$  (the uncoated *Rogers RO4003C* substrate used before), but for different vertical distances (air gap,  $g$ ) with regard to the sensing line. Note that this is equivalent to modify the dielectric constant of a hypothetical semi-infinite MUT in contact with the sensing line. Such equivalent dielectric constant,  $\epsilon_{MUT,eq}$ , can be estimated by simulation. For that purpose we have simulated the structure by considering

different air gaps in the interval from  $g = 0$  mm to  $g = 3$  mm (far enough so as to consider that the electromagnetic field generated by the line does not reach the MUT). From the output variable,  $\Delta\phi_\rho$ , resulting for each air gap distance (Fig. 8), the equivalent dielectric constant,  $\epsilon_{MUT,eq}$ , can be determined by reading it from Fig. 7 (i.e., using the simulated phase variation of Fig. 8, Fig. 7 provides  $\epsilon_{MUT,eq}$  for each simulated point). Thus, we can generate a correspondence between the air gap  $g$ , and the equivalent dielectric constant  $\epsilon_{MUT,eq}$ . Such dependence is given in the inset of Fig. 9, where the phase dependence with  $\epsilon_{MUT,eq}$  for the experimental data (squared symbols) and with  $\epsilon_{MUT}$  for the simulations is depicted. The agreement is reasonably good taking into account the difficulty in controlling the air gap distance for small values. In addition, in this experiment, similar to the previous experimental campaigns, two slabs have been stacked up. By screwing the whole MUT against the sensing region, as done in the previous measurements, the presence of a thin air layer between the slabs is minimized. However, this has not been done in the measurements of Fig. 8, because the MUT is not in contact with the sensing region.

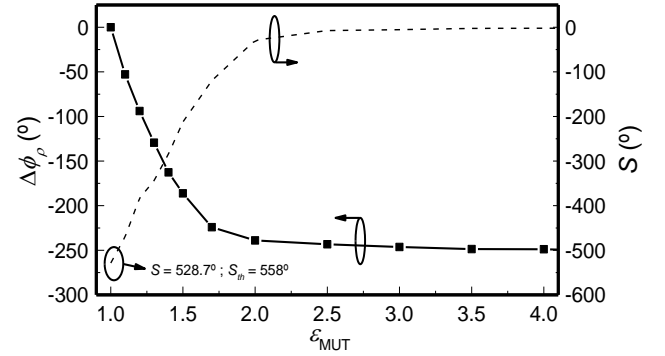


Fig. 7. Simulated phase of the reflection coefficient for different values of  $\epsilon_{MUT}$  for the sensor of Fig. 6, and simulated sensitivity. The theoretical sensitivity, designated as  $S_{th}$ , is also indicated. The sensitivities in the limit of small perturbations are given in absolute value.

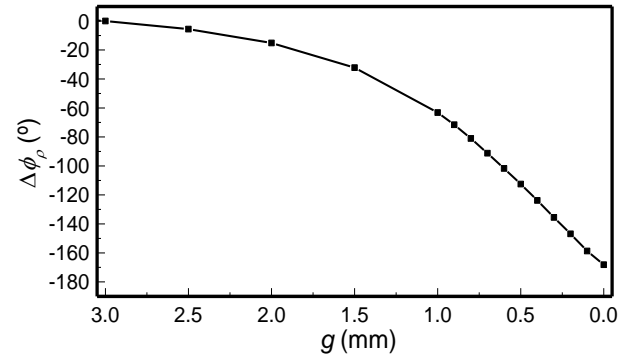


Fig. 8. Measured phase of the reflection coefficient for the sensor of Fig. 6, by loading the sensing region with a MUT separated a variable distance  $g$ . The considered MUT is the uncoated *Rogers RO4003C* with thickness  $h = 3$  mm and dielectric constant  $\epsilon_{MUT} = 3.55$ .

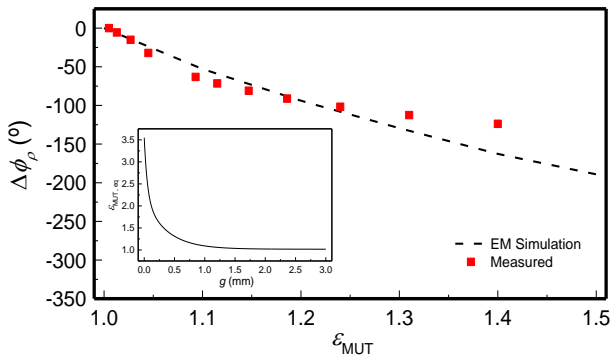


Fig. 9. Measured phase of the reflection coefficient for the sensor of Fig. 6, by loading the sensing region with a MUT separated a variable distance  $g$ . The considered MUT is the uncoated *Rogers RO4003C* with thickness  $h = 3$  mm (two stacked slabs) and dielectric constant  $\epsilon_{MUT} = 3.55$ . The equivalent dielectric constant for the measured data is given by  $g$ , according to the correspondence curve shown in the inset. For the simulated data, the horizontal axis is the dielectric constant of a hypothetical semi-infinite MUT in contact with the sensing region. In other words, the simulated curve is the one of Fig. 7, but restricted to a smaller range.

Nevertheless, the sensor is able to detect tiny variations of  $\epsilon_{MUT,eq}$  in the vicinity of  $\epsilon_{MUT,eq} = 1$ , corresponding to air gap separations close to 3 mm. This experiment, emulating low perturbations in the dielectric constant of the MUT in the highly sensitive region, validates the structure of Fig. 6 as a sensor exhibiting very high sensitivity with relatively small sensing region.

The results of these section and those of Section IV are indicative of the huge potential of these step-impedance transmission line reflective-mode phase-variation sensors for sensitivity enhancement, without the need to consider large sensing areas (or MUTs). Comparison of the reported phase-variation sensors with other sensors devoted to dielectric characterization is not easy, since there are few sensors available in the literature whose working principle is phase variation. In [20],[25], the reported phase-variation sensors are based on long (uniform) sensing lines (meandered in [25]), in order to achieve high sensitivity. In [25], the sensitivity of the sensor (a differential-mode sensor operating in transmission) is very good ( $S = 415.6^\circ$ ), but at the expense of a pair of meandered lines of length 67.03 cm (the reported sensitivity of the sensor of [20] is worse, i.e.,  $S = 54.85^\circ$ ). Moreover, the sensing area for the MUT in the sensor of [25] is as large as  $105.56 \text{ cm}^2$ . By contrast, the sensing area of the sensor reported in this section (Fig. 6) is  $15.08 \text{ cm}^2$ , and the reported sensitivity is as high as  $528.7^\circ$  (simulated). This combination of sensitivity and sensing area is very competitive. Moreover, the sensitivity can be further enhanced (maintaining the sensing region unaltered) by simply considering additional sections, as indicated before (this interesting property is not present in the sensors reported in [20],[25]). It should also be mentioned that the sensing region of the device can actually be made much smaller, since a width of few times the width of the sensing line suffices.

There are other sensors available in the literature where the working principle is phase variation, but the output variable is not the phase [17],[27],[28]. In the recent paper [28], it was demonstrated that by combining a pair of mirrored meandered lines with a double rat-race structure conveniently designed, the sensitivity of the differential sensor can be enhanced (in that sensor, the output variable is

the magnitude of the transmission coefficient of the resulting two-port device). Nevertheless, the sensitivity enhancement capability of the strategy proposed in this work is by far superior to the one of [28]. In [17] and [27], the reported sensors are also based on phase variation, although the output variable is not the phase, but the magnitude of the transmission coefficient [17], or the magnitude of the cross-mode transmission coefficient [27]. The sensitivity of such sensors [17],[27] is high, thanks to the strong dispersion of the considered sensing lines (left handed lines in [17] and electro-inductive-wave transmission lines in [27]). It is especially remarkable the sensitivity of the sensor in [17], but at the expense of a relatively large sensing area (not given in [17]). However, further increasing the sensitivity requires the elongation of the sensing lines in both sensors. Moreover, the robustness of these sensors against fabrication related tolerances is limited since either defect ground structures, vias, or other elements loading the lines are needed. By contrast, the phase-variation sensors reported in this paper are implemented by a mere cascade of alternating high/low impedance transmission line sections. A comparison of these sensors is summarized in Table I.

TABLE I  
COMPARISON OF VARIOUS SENSORS BASED ON PHASE VARIATION

Ref.	Maximum Sensitivity*	Resolution**	Size***	Frequency
[17]	600 dB	0.0017	N.A.	2.3 GHz
[20]	$54.85^\circ$	0.0911	$2.5 \text{ cm}^2$	10 GHz
[25]	$415.6^\circ$	0.0120	$105.6 \text{ cm}^2$	6 GHz
[27]	25.33 dB	0.0395	$44.55 \text{ cm}^2$	4.6 GHz
[28]	17.62 dB	0.0560	$1.2 \text{ cm}^2$	2 GHz
<b>Proposed design (Fig. 6)</b>	<b><math>528.7^\circ</math></b>	<b>0.0095</b>	<b><math>15.08 \text{ cm}^2</math></b>	<b>2 GHz</b>

\*Units are degrees for sensors where the output variable is a phase, and units are dB for sensors where the output variable is a transmission coefficient.

\*\*The resolution in the dielectric constant is calculated by assuming that either  $5^\circ$  or 1dB in the output variable (depending on the case) can be discriminated.

\*\*\*The size corresponds to the sensing area.

In summary, the reported sensors exhibit a good combination of size (sensing region) and performance (sensitivity), they operate at a single frequency, they are based on a reflective-mode one-port structure, and, most important, the sensitivity, the key sensor parameter, can be enhanced at wish, keeping unaltered the region devoted to the MUT. This later aspect is very relevant and a unique feature of the reported sensors. Moreover, the part of the sensors excluding the sensing region is as simple as a stepped impedance transmission line consisting of cascaded quarter-wavelength transmission line sections. As it has been shown, few sections suffice to achieve very high sensitivity.

## VI. CONCLUSIONS

In conclusion, a strategy to significantly enhance the sensitivity of reflective-mode phase-variation sensors based on open-ended lines has been reported in this paper. From a detailed sensitivity analysis, it is demonstrated that by considering a step-impedance discontinuity, with the sensing region comprising the space between the discontinuity and the open end, the sensitivity can be engineered. It is concluded from such analysis that for sensitivity

enhancement, the electrical length of the sensing line must be either a multiple of  $180^\circ$ , or an odd multiple of  $90^\circ$ , whereas the line present between the discontinuity and the input port (design line) should exhibit a phase of  $90^\circ$  (or an odd multiple). Moreover, sensitivity is enhanced by impedance contrast. Particularly, high impedance sensing line and low impedance design line is a necessary condition for sensitivity optimization in sensors with  $90^\circ$  sensing lines, whereas in sensors with  $180^\circ$  sensing lines, the impedance contrast should be the opposite one. For validation purposes, a first set of six prototype sensors has been fabricated. Two of them exhibit a step-impedance discontinuity and have been designed following the design guidelines of the theoretical analysis. In two sensors, a uniform mismatched sensing line (with high impedance in one case and low impedance in the other one) has been considered. Finally, the other sensors have been implemented by means of uniform  $90^\circ$  and  $180^\circ$  matched lines. In all these sensors, the variation of the phase of the reflection coefficient (the output variable) with the dielectric constant of the material under test (MUT) has been inferred by considering different dielectric slabs. The sensor sensitivity, the key parameter, has been inferred from simulations, since a large number of data points is required for the accurate determination of such parameter. From the results, it is concluded that the proposed strategy, based on the step-impedance discontinuity, is very useful for the implementation of highly sensitive phase-variation sensors. In the last part of the paper, it has been demonstrated that the sensitivity can further be enhanced by simply cascading further quarter-wavelength transmission line sections with alternating high and low impedance. By this means, the sensitivity can be increased at wish, maintaining the sensing region unaltered. This is an essential and unique property of these phase-variation sensors. The sensitivity achieved in the last designed and fabricated prototype, based on three quarter-wavelength step-impedance transmission line sections (including the sensing line section), is  $S = 528.7^\circ$ . This is 56.2 times larger than the sensitivity achieved in the reflective-mode phase-variation sensor based on an ordinary and matched line with identical sensing line length. These sensors may be of special interest in applications related to the measurement of small changes in the dielectric constant of the MUT, including determination of material composition of solids and liquids (e.g. concentration of solute in very diluted solutions), detection of defects in samples (as compared to a reference), sensing and monitoring of industrial processes (e.g., wine fermentation), etc. These applications are left for future works. In the present paper, the main objective has been to demonstrate the potential of these step-impedance reflective-mode phase-variation sensors for sensitivity optimization, on the basis of a detailed sensitivity analysis, validated through simulation and simple experiments.

#### APPENDIX A EXACT CALCULATION OF THE SENSITIVITY

Actually, the variation of  $\varepsilon_{MUT}$  modifies both the phase,  $\phi_s$ , and the characteristic impedance,  $Z_s$ , of the sensing line. Therefore, the sensitivity of the phase of the reflection

coefficient,  $\phi_\rho$ , with  $\varepsilon_{MUT}$  should be expressed as

$$S = \frac{d\phi_\rho}{d\varepsilon_{MUT}} = \frac{d\phi_\rho}{d\phi_s} \cdot \frac{d\phi_s}{d\varepsilon_{MUT}} + \frac{d\phi_\rho}{dZ_s} \cdot \frac{dZ_s}{d\varepsilon_{MUT}} \quad (A1)$$

However, by including the last term of the right-hand side member of (A1), the phase and impedance conditions for sensitivity optimization are roughly the same as those give in the body of the text. Specifically, for the structure based only on the sensing line, the sensitivity is optimized when the phase of such line is either  $\phi_s = n \cdot \pi$  (with  $Z_s$  low), or  $\phi_s = (2n + 1) \cdot \pi/2$  (with  $Z_s$  high), with  $n = 0, 1, 2, \dots$ . Moreover, under such phase conditions, the derivative  $d\phi_\rho/dZ_s$  is null. Hence, the sensitivity given by (4) provides an accurate result as far as it is calculated for the optimum phase conditions. Indeed, for the different structures considered in this paper, the phase conditions that optimize  $d\phi_\rho/d\phi_s$  are those that null  $d\phi_\rho/dZ_s$ . Consequently, the exhaustive study focused on  $d\phi_\rho/d\phi_s$  optimization, conducted in Section III and generalized in Section V, is fully justified. Let us next demonstrate the previous assertions for the structure based simply on the sensing line (and considering implementation in microstrip technology).

The two terms of the first product in (A1) are given by (8) and (28), but they can be alternatively expressed as:

$$\frac{d\phi_\rho}{d\phi_s} = -\frac{2\frac{Z_s}{Z_0}\sin^{-2}\phi_s}{1+(\frac{Z_s}{Z_0})^2\cot^2\phi_s} \quad (A2)$$

$$\frac{d\phi_s}{d\varepsilon_{MUT}} = \frac{\phi_s}{4\varepsilon_{eff}}(1-F) \quad (A3)$$

The two terms of the second product are easily inferred from (7) and from the expression providing the characteristic impedance of a microstrip line, i.e.,

$$\frac{d\phi_\rho}{dZ_s} = \frac{2}{1+(\frac{Z_s}{Z_0})^2\cot^2\phi_s} \cdot \frac{\cot\phi_s}{Z_0} \quad (A4)$$

$$\frac{dZ_s}{d\varepsilon_{MUT}} = \frac{dZ_s}{d\varepsilon_{eff}} \frac{d\varepsilon_{eff}}{d\varepsilon_{MUT}} = -\frac{Z_s}{4\varepsilon_{eff}}(1-F) \quad (A5)$$

Introducing (A2)-(A5) in (A1), the sensitivity is found to be

$$S = -\frac{Z_s(1-F)}{2Z_0\varepsilon_{eff}} \cdot \frac{\phi_s\sin^{-2}\phi_s + \cot\phi_s}{1+(\frac{Z_s}{Z_0})^2\cot^2\phi_s} \quad (A6)$$

Let us now calculate the derivative of (A6) with respect to  $\phi_s$ , in order to obtain the values of  $\phi_s$  that maximize the sensitivity. After some algebra, one obtains

$$\frac{dS}{d\phi_s} = -\frac{Z_s(1-F)\sin^{-2}\phi_s}{Z_0\varepsilon_{eff}} \cdot \frac{\cot\phi_s\left\{\left(\frac{Z_s}{Z_0}\right)^2\cot\phi_s + \phi_s\left(\frac{Z_s}{Z_0}\right)^2 - \phi_s\right\}}{\left(1+(\frac{Z_s}{Z_0})^2\cot^2\phi_s\right)^2} \quad (A7)$$

It is apparent that  $\phi_s = (2n + 1) \cdot \pi/2$  nulls (A7). For such phase of the sensing line, the sensitivity (A6) is

$$S = -\frac{Z_s(1-F)}{2Z_0\varepsilon_{eff}} \phi_s \quad (A8)$$

This value is identical to the one inferred from (4), using (10b) and (28), and for such phase value the line impedance  $Z_s$  must be high in order to obtain high sensitivity. By contrast, for  $\phi_s = n \cdot \pi$ , equation (A7) is not strictly null. There is, however, an additional condition that nulls (A7), i.e.,

$$\phi_s \tan\phi_s = \frac{Z_s^2}{Z_0^2 - Z_s^2} \quad (A9)$$

and the solution of (A9) can be approximated by  $\phi_s = n\pi$  as far as  $Z_s < Z_0$ . Thus, it can be concluded that for  $Z_s < Z_0$  there is a maximum of the sensitivity very close to  $\phi_s = n\pi$ . Consequently, it is reasonable to set the phase of the sensing line to such value for low impedance sensing lines. For  $\phi_s = n\pi$ , the sensitivity is

$$S = -\frac{Z_0(1-F)}{2Z_s\epsilon_{eff}} \phi_s \quad (\text{A10})$$

also given by (4), but in this case utilizing (10a) and (28). For both phases,  $\phi_s = n\pi$  and  $\phi_s = (2n+1)\pi/2$ , equation (A4) is null and, for that reason, the sensitivity can be calculated using the simplified expression (4).

Despite the fact that the previous analysis has been carried out on the basis of the structure of Section III.A, for the structure of Section III.B, consisting of the sensing line plus an additional (design) line, a similar behavior occurs. Namely, for the optimum phase conditions, summarized in Section III.B, the derivative  $d\phi_p/dZ_s$  is also null, and therefore the sensitivity can be calculated according to (4). Let us demonstrate this by calculating such derivative from (13). After some simple calculation, the following result is obtained:

$$\frac{d\phi_p}{dZ_s} = \frac{2Z_0Z^2 \cot \phi_s (1+\tan^2 \phi)}{Z_0^2(Z + Z_s \tan \phi \cot \phi_s)^2 + Z^2(Z_s \cot \phi_s - Z \tan \phi)^2} \quad (\text{A11})$$

and it follows that  $d\phi_p/dZ_s = 0$  for  $\phi = (2n+1)\pi/2$  and  $\phi_s = n\pi$  or  $\phi_s = (2n+1)\pi/2$  (the optimum phase conditions according to the analysis of Section III.B). This applies also to the generalized structure, with an arbitrary number of cascaded high/low impedance design lines with  $\phi_i = (2n+1)\pi/2$ .

Obviously, the calculation of the sensitivity for phases different than those corresponding to the optimum values [i.e.,  $\phi_i = (2n+1)\pi/2$  and  $\phi_s = n\pi$  or  $\phi_s = (2n+1)\pi/2$ ] would require the use of (A1), rather than (4). Nevertheless, the paper is entirely focused on sensitivity optimization for small perturbations (representing small variations of the phase of the sensing line around the optimum value). For this reason, the analysis of Section III, generalized in Section V, is justified. Indeed, the good agreement between the theoretical sensitivities for small perturbations, inferred from (4), and those calculated from the simulated data when  $\epsilon_{MUT} \rightarrow 1$  (see Figs. 5 and 7) validate the theory.

## APPENDIX B

### EFFECTS OF LOSSES ON SENSOR SENSITIVITY

Let us evaluate  $S_{\phi_s}$  by considering the effects of losses in the MUT (to a first-order approximation, the ohmic losses of the step-impedance transmission line, as well as the dielectric losses of the substrate, can be neglected, provided the considered substrate is a low-loss material). The impedance seen from the step-impedance discontinuity adjacent to the sensing line,  $Z_{in,s}$ , is no longer given by equation (5), since the complex propagation constant,  $\gamma$ , must be considered in order to account for the effects of the lossy MUT. Thus, such impedance is given by

$$Z_{in,s} = Z_s \coth \gamma l_s \quad (\text{B.1})$$

where  $\gamma = \alpha + j\beta$ , and  $\alpha$  and  $\beta$  are the attenuation constant and the phase constant, respectively, of the sensing line. After some simple algebra, (B.1) can be expressed as

$$Z_{in,s} = Z_s \frac{\sinh 2\alpha l_s - j \sin 2\phi_s}{\cosh 2\alpha l_s - \cos 2\phi_s} \quad (\text{B.2})$$

with  $\phi_s = \beta l_s$ . The impedance seen from the input port of the whole sensor,  $Z_{in,N}$ , is calculated by means of (31), with  $Z_{in,s}$  given by (B.2). The reflection coefficient is thus

$$\rho = \frac{\left( Z_s \frac{\sinh 2\alpha l_s - j \sin 2\phi_s}{\cosh 2\alpha l_s - \cos 2\phi_s} \right)^{(-1)^N} \cdot \Pi - Z_0}{\left( Z_s \frac{\sinh 2\alpha l_s - j \sin 2\phi_s}{\cosh 2\alpha l_s - \cos 2\phi_s} \right)^{(-1)^N} \cdot \Pi + Z_0} \quad (\text{B.3})$$

where  $\Pi$  is the product operator defined in (31) with the argument omitted, for simplicity. At this point, in order to calculate the phase of the reflection coefficient by considering losses, it is convenient to distinguish between even- and odd-order structures. For  $N$  even, the reflection coefficient can be expressed as

$$\rho = \frac{Z_s \Pi (\sinh 2\alpha l_s - j \sin 2\phi_s) - Z_0 (\cosh 2\alpha l_s - \cos 2\phi_s)}{Z_s \Pi (\sinh 2\alpha l_s - j \sin 2\phi_s) + Z_0 (\cosh 2\alpha l_s - \cos 2\phi_s)} \quad (\text{B.4})$$

and the phase of the reflection coefficient is

$$\phi_\rho = \arctan \left( \frac{Z_s \Pi \sin 2\phi_s}{Z_0 (\cosh 2\alpha l_s - \cos 2\phi_s) - Z_s \Pi \sinh 2\alpha l_s} \right) + \arctan \left( \frac{Z_s \Pi \sin 2\phi_s}{Z_0 (\cosh 2\alpha l_s - \cos 2\phi_s) + Z_s \Pi \sinh 2\alpha l_s} \right) \quad (\text{B.5})$$

The sensitivity with the phase of the sensing line is therefore

$$S_{\phi_s} = F \cdot \frac{2Z_s \Pi \cos 2\phi_s (Z_0 (\cosh 2\alpha l_s - \cos 2\phi_s) - Z_s \Pi \sinh 2\alpha l_s) - 2Z_s Z_0 \Pi (\sin 2\phi_s)^2}{(Z_0 (\cosh 2\alpha l_s - \cos 2\phi_s) - Z_s \Pi \sinh 2\alpha l_s)^2} + F' \cdot \frac{2Z_s \Pi \cos 2\phi_s (Z_0 (\cosh 2\alpha l_s - \cos 2\phi_s) + Z_s \Pi \sinh 2\alpha l_s) - 2Z_s Z_0 \Pi (\sin 2\phi_s)^2}{(Z_0 (\cosh 2\alpha l_s - \cos 2\phi_s) + Z_s \Pi \sinh 2\alpha l_s)^2} \quad (\text{B.6})$$

where the factors  $F$  and  $F'$  defined as

$$F = \frac{1}{1+(X)^2} \quad (\text{B.7a})$$

$$F' = \frac{1}{1+(X')^2} \quad (\text{B.7b})$$

have been introduced for simplicity. In (B.7),  $X$  and  $X'$  are the arguments of the arctan in the first and second term of the right hand side member of expression (B.5).

For  $N$  odd, the reflection coefficient is found to be

$$\rho = \frac{-Z_0 (\sinh 2\alpha l_s - j \sin 2\phi_s) + Z_s^{-1} \Pi (\cosh 2\alpha l_s - \cos 2\phi_s)}{Z_0 (\sinh 2\alpha l_s - j \sin 2\phi_s) + Z_s^{-1} \Pi (\cosh 2\alpha l_s - \cos 2\phi_s)} \quad (\text{B.8})$$

and the phase of the reflection coefficient is

$$\phi_\rho = \arctan \left( \frac{Z_0 \sin 2\phi_s}{Z_s^{-1} \Pi (\cosh 2\alpha l_s - \cos 2\phi_s) - Z_0 \sinh 2\alpha l_s} \right) + \arctan \left( \frac{Z_0 \sin 2\phi_s}{Z_s^{-1} \Pi (\cosh 2\alpha l_s - \cos 2\phi_s) + Z_0 \sinh 2\alpha l_s} \right) \quad (\text{B.9})$$

Taking the derivative of (B.9), the sensitivity is obtained, i.e.,

$$S_{\phi_s} = F \cdot \frac{2Z_0 \cos 2\phi_s (Z_s^{-1} \Pi (\cosh 2\alpha l_s - \cos 2\phi_s) - Z_0 \sinh 2\alpha l_s) - 2Z_0 Z_s^{-1} \Pi (\sin 2\phi_s)^2}{(Z_s^{-1} \Pi (\cosh 2\alpha l_s - \cos 2\phi_s) - Z_0 \sinh 2\alpha l_s)^2} + F' \cdot \frac{2Z_0 \cos 2\phi_s (Z_s^{-1} \Pi (\cosh 2\alpha l_s - \cos 2\phi_s) + Z_0 \sinh 2\alpha l_s) - 2Z_0 Z_s^{-1} \Pi (\sin 2\phi_s)^2}{(Z_s^{-1} \Pi (\cosh 2\alpha l_s - \cos 2\phi_s) + Z_0 \sinh 2\alpha l_s)^2} \quad (\text{B.10})$$

with  $F$  and  $F'$  given by (B.7), and  $X$  and  $X'$  corresponding to the arguments of the arctan of the first and second term of the right hand side member of (B.9), respectively.

If we now consider the two optimum phases of the sensing line for sensitivity optimization, four cases (similar to those enumerated in Section V) arise:

- Case A':  $\phi_s = (2n + 1)\cdot\pi/2$  and  $N$  odd. Evaluation of (B.10) gives:

$$S_{\phi_s} = -\frac{2Z_0}{Z_s^{-1}\Pi(\cosh 2\alpha l_s + 1)} \cdot \left\{ \frac{1}{1 - \frac{Z_0 \sinh 2\alpha l_s}{Z_s^{-1}\Pi(\cosh 2\alpha l_s + 1)}} + \frac{1}{1 + \frac{Z_0 \sinh 2\alpha l_s}{Z_s^{-1}\Pi(\cosh 2\alpha l_s + 1)}} \right\} \quad (\text{B.11})$$

For moderate and low-loss materials (i.e., satisfying  $\alpha l_s \ll 1$ ), (B.11) can be approximated by

$$S_{\phi_s} = -\frac{2Z_0}{Z_s^{-1}\Pi(1 + \alpha^2 l_s^2)} \quad (\text{B.12})$$

where it has been assumed that  $\sinh(2\alpha l_s) \approx 2\alpha l_s$  and  $\cosh(2\alpha l_s) \approx 1 + 2\alpha^2 l_s^2$ .

- Case B':  $\phi_s = n\cdot\pi$  and  $N$  odd. In this case, the sensitivity (using B.10) is found to be

$$S_{\phi_s} = \frac{2Z_0}{Z_s^{-1}\Pi(\cosh 2\alpha l_s - 1) - Z_0 \sinh 2\alpha l_s} + \frac{2Z_0}{Z_s^{-1}\Pi(\cosh 2\alpha l_s - 1) + Z_0 \sinh 2\alpha l_s} \quad (\text{B.13})$$

and the result for the low-loss approximation can be expressed as

$$S_{\phi_s} = \frac{Z_0}{Z_s^{-1}\Pi\alpha^2 l_s^2 - Z_0 \alpha l_s} + \frac{Z_0}{Z_s^{-1}\Pi\alpha^2 l_s^2 + Z_0 \alpha l_s} = \frac{2Z_0 Z_s^{-1}\Pi}{Z_s^{-2}\alpha^2 l_s^2 \Pi^2 - Z_0^2} \quad (\text{B.14})$$

- Case C':  $\phi_s = (2n + 1)\cdot\pi/2$  and  $N$  even. Evaluation of (B.6) provides

$$S_{\phi_s} = -\frac{2Z_s \Pi}{Z_0(\cosh 2\alpha l_s + 1)} \cdot \left\{ \frac{1}{1 - \frac{Z_s \Pi \sinh 2\alpha l_s}{Z_0(\cosh 2\alpha l_s + 1)}} + \frac{1}{1 + \frac{Z_s \Pi \sinh 2\alpha l_s}{Z_0(\cosh 2\alpha l_s + 1)}} \right\} \quad (\text{B.15})$$

and the following result is obtained for the low-loss approximation:

$$S_{\phi_s} = -\frac{2Z_s \Pi}{Z_0(1 + \alpha^2 l_s^2)} \quad (\text{B.16})$$

- Case D':  $\phi_s = n\cdot\pi$  and  $N$  even. In this case, (B.6) is

$$S_{\phi_s} = \frac{2Z_s \Pi}{Z_0(\cosh 2\alpha l_s - 1) - Z_s \Pi \sinh 2\alpha l_s} + \frac{2Z_s \Pi}{Z_0(\cosh 2\alpha l_s - 1) + Z_s \Pi \sinh 2\alpha l_s} \quad (\text{B.17})$$

and the result for the low-loss approximation can be expressed as

$$S_{\phi_s} = \frac{Z_s \Pi}{Z_0 \alpha^2 l_s^2 - \alpha Z_s \Pi} + \frac{Z_s \Pi}{Z_0 \alpha^2 l_s^2 + \alpha Z_s \Pi} = \frac{2Z_0 Z_s \Pi}{Z_0^2 \alpha^2 l_s^2 - Z_s^2 \Pi^2} \quad (\text{B.18})$$

Inspection of expressions (B.12), (B.14), (B.16) and (B.18) reveals that losses do not alter so much the sensitivity, as compared to the lossless case, provided the low-loss approximation is satisfied ( $\alpha l_s \ll 1$ ). The reason is that the term that accounts for losses ( $\alpha l_s$ ) appears squared in those equations. Consequently, its contribution to the sensitivity is small. Indeed, in the limit  $\alpha l_s \rightarrow 0$ , the sensitivities (B.12), (B.14), (B.16) and (B.18) are simplified to those given by expressions (36) of Section V, corresponding to the lossless cases (as expected).

Since the sensitivity has been evaluated at specific values of the phase of the sensing line [ $\phi_s = (2n + 1)\cdot\pi/2$  and  $\phi_s = n\cdot\pi$ ], it is also convenient to directly compare the output

variable of the considered sensors,  $\phi_\rho$ , for the lossless and low-loss approximation cases. For  $N$  even, expression (B.5), with  $\sinh(2\alpha l_s) \approx 2\alpha l_s$  and  $\cosh(2\alpha l_s) \approx 1 + 2\alpha^2 l_s^2$ , provides

$$\phi_\rho = \arctan\left(\frac{Z_s \Pi \sin 2\phi_s}{Z_0(1 - \cos 2\phi_s)\left\{1 + \frac{2\alpha l_s(Z_0 \alpha l_s - Z_s \Pi)}{Z_0(1 - \cos 2\phi_s)}\right\}}\right) + \arctan\left(\frac{Z_s \Pi \sin 2\phi_s}{Z_0(1 - \cos 2\phi_s)\left\{1 + \frac{2\alpha l_s(Z_0 \alpha l_s + Z_s \Pi)}{Z_0(1 - \cos 2\phi_s)}\right\}}\right) \quad (\text{B.19})$$

and such expression can be further approximated by

$$\phi_\rho = 2\arctan\left(\frac{Z_s \Pi}{Z_0} \cot \phi_s\right) - \frac{\frac{Z_s \Pi}{Z_0} \cot \phi_s}{1 + \left(\frac{Z_s \Pi}{Z_0} \cot \phi_s\right)^2} \cdot \frac{4\alpha^2 l_s^2}{(1 - \cos 2\phi_s)} \quad (\text{B.20})$$

where the first-order Taylor expansion  $\arctan[A/(1+x)] = \arctan[A] - Ax/(1+A^2)$ , with  $x$  small, and the trigonometric identity  $\sin(2\phi_s)/(1 - \cos 2\phi_s) = \cot \phi_s$  have been used. For  $N$  odd, following a similar procedure, the phase of the reflection coefficient can be approximated by

$$\phi_\rho = 2\arctan\left(\frac{Z_s Z_0}{\Pi} \cot \phi_s\right) - \frac{\frac{Z_s Z_0}{\Pi} \cot \phi_s}{1 + \left(\frac{Z_s Z_0}{\Pi} \cot \phi_s\right)^2} \cdot \frac{4\alpha^2 l_s^2}{(1 - \cos 2\phi_s)} \quad (\text{B.21})$$

As it can be appreciated, if losses are small, the phase of the reflection coefficient does not significantly change as compared to the lossless case (note that, again, the lossy term,  $\alpha l_s$ , appears squared). Moreover, (B.20) and (B.21) coincide with expression (34) in the limit  $\alpha l_s \rightarrow 0$ , as expected.

Indeed, for low-loss MUTs, it can be concluded from (B.20) and (B.21) that the phase of the reflection coefficient,  $\phi_\rho$ , does not depend on the attenuation constant of the sensing line,  $\alpha$  (in turn related to the loss factor of the MUT). Moreover, it is well known that if losses are small, the phase constant of the sensing line,  $\beta$ , is uniquely determined by the effective dielectric constant of that line [43]. Therefore, the output variable of the proposed sensor,  $\phi_\rho$ , can be used for the determination of the dielectric constant of the MUT, despite the presence of losses (provided losses are small).

To end this appendix, it is worth-mentioning that from the measurement of the reflection coefficient at the operating frequency (including not only the phase, but also the modulus), it is possible to infer the attenuation constant of the sensing line,  $\alpha$ . It can be isolated from (B.4) or (B.8), depending on whether  $N$  is even or odd, as far as  $\rho$  is inferred from measurement, and  $\phi_s$  can be obtained from (34). From the attenuation constant, it is possible to obtain the loss tangent of the MUT, e.g., from a calibration curve inferred from MUTs with well-known loss factor. Nevertheless, this aspect is out of the scope of this paper, since for the measurement of the loss factor of the MUT, in general, resonant methods are preferred.

## REFERENCES

- [1] M. Puentes, C. Weiß, M. Schübler, and R. Jakoby, "Sensor array based on split ring resonators for analysis of organic tissues," in *IEEE MTT-S Int. Microw. Symp.*, Baltimore, MD, USA, Jun. 2011, pp. 1-4.
- [2] B. Ebrahimi, W. Withayachumnankul, S. Al-Sarawi, D. Abbott, "High-sensitivity metamaterial-inspired sensor for microfluidic dielectric characterization," *IEEE Sensors J.*, vol. 14, no. 5, pp. 1345-1351, May 2014

- [3] M. Schüßler, C. Mandel, M. Puentes, and R. Jakoby, "Metamaterial inspired microwave sensors," *IEEE Microw. Mag.*, vol. 13, no. 2, pp. 57–68, Mar. 2012.
- [4] M. S. Boybay and O. M. Ramahi, "Material characterization using complementary split-ring resonators," *IEEE Trans. Instrum. Meas.*, vol. 61, no. 11, pp. 3039–3046, Nov. 2012.
- [5] C.-S. Lee and C.-L. Yang, "Complementary split-ring resonators for measuring dielectric constants and loss tangents," *IEEE Microw. Wireless Compon. Lett.*, vol. 24, no. 8, pp. 563–565, Aug. 2014.
- [6] C.-L. Yang, C.-S. Lee, K.-W. Chen, and K.-Z. Chen, "Noncontact measurement of complex permittivity and thickness by using planar resonators," *IEEE Trans. Microw. Theory Techn.*, vol. 64, no. 1, pp. 247–257, Jan. 2016.
- [7] L. Su, J. Mata-Contreras, P. Vélez, F. Martín, "Estimation of the complex permittivity of liquids by means of complementary split ring resonator (CSRR) loaded transmission lines", *2017 IEEE MTT-S International Microwave Workshop Series on Advanced Materials and Processes (IMWS-AMP 2017)*, Pavia, Italy, 20–22 Sep. 2017.
- [8] L. Su, J. Mata-Contreras, P. Vélez, B. Fernández-Prieto and F. Martín, "Analytical method to estimate the complex permittivity of oil Samples", *Sensors*, 18(4), paper 984, 2018.
- [9] B.K. Jha, N. Delmonte, A. Lamecki, M. Mrozowski, M. Bozzi, "Design of microwave-based angular displacement sensor", *IEEE Microw. Wireless Compon. Lett.*, vol. 29 (4), pp. 306–308, Apr. 2019.
- [10] B. K. Horestani, J. Naqui, Z. Shaterian, D. Abbott, C. Fumeaux, and F. Martín, "Two-dimensional alignment and displacement sensor based on movable broadside-coupled split ring resonators," *Sensors and Actuators A*, vol. 210, pp. 18–24, Apr. 2014.
- [11] J. Naqui, *et al.*, "Transmission lines loaded with pairs of magnetically coupled stepped impedance resonators (SIRs): modeling and application to microwave sensors," *IEEE MTT-S Int. Microwave Symp.*, Tampa, FL, USA, Jun. 2014, pp. 1–4.
- [12] L. Su, J. Naqui, J. Mata-Contreras, and F. Martín "Modeling metamaterial transmission lines loaded with pairs of coupled split ring resonators," *IEEE Ant. Wireless Propag. Lett.*, vol. 14, pp. 68–71, 2015.
- [13] L. Su, J. Naqui, J. Mata-Contreras, and F. Martín, "Modeling and applications of metamaterial transmission lines loaded with pairs of coupled complementary split ring resonators (CSRRs)," *IEEE Ant. Wireless Propag. Lett.*, vol. 15, pp. 154–157, 2016.
- [14] L. Su, J. Mata-Contreras, J. Naqui, and F. Martín, "Splitter/combiner microstrip sections loaded with pairs of complementary split ring resonators (CSRRs): modeling and optimization for differential sensing applications," *IEEE Trans. Microw. Theory Techn.*, vol. 64, pp. 4362–4370, Dec. 2016.
- [15] B. Ebrahimi, J. Scott and K. Ghorbani, "Differential sensors using microstrip lines loaded with two split ring resonators," *IEEE Sensors J.*, vol. 18, pp. 5786–5793, Jul. 2018.
- [16] P. Vélez, L. Su, K. Grenier, J. Mata-Contreras, D. Dubuc, and F. Martín, "Microwave microfluidic sensor based on a microstrip splitter/combiner configuration and split ring resonators (SRR) for dielectric characterization of liquids", *IEEE Sensors J.*, vol. 17, pp. 6589–6598, Oct. 2017.
- [17] C. Damm, M. Schussler, M. Puentes, H. Maune, M. Maasch and R. Jakoby, "Artificial transmission lines for high sensitive microwave sensors," *IEEE Sensors Conf.*, Christchurch, New Zealand, pp.755–758, Oct. 2009.
- [18] M. Schuessler, C. Mandel, M. Puentes and R. Jakoby, "Metamaterial inspired microwave sensors," *IEEE Microw. Mag.*, vol. 13, no. 2, pp. 57–68, Mar. 2012.
- [19] P. Vélez, J. Mata-Contreras, L. Su, D. Dubuc, K. Grenier, F. Martín, "Modeling and Analysis of Pairs of Open Complementary Split Ring Resonators (OCSRRs) for Differential Permittivity Sensing", *2017 IEEE MTT-S International Microwave Workshop Series on Advanced Materials and Processes (IMWS-AMP 2017)*, Pavia, Italy, 20–22 September 2017.
- [20] F.J. Ferrández-Pastor, J.M. García-Chamizo and M. Nieto-Hidalgo, "Electromagnetic differential measuring method: application in microstrip sensors developing", *Sensors*, vol. 17, p. 1650, 2017.
- [21] P. Vélez, K. Grenier, J. Mata-Contreras, D. Dubuc and F. Martín, "Highly-Sensitive Microwave Sensors Based on Open Complementary Split Ring Resonators (OCSRRs) for Dielectric Characterization and Solute Concentration Measurement in Liquids", *IEEE Access*, vol. 6, pp. 48324–48338, Aug. 2018.
- [22] B. Ebrahimi, J. Scott, K. Ghorbani, "Transmission Lines Terminated With LC Resonators for Differential Permittivity Sensing", *IEEE Microw. Wireless Compon. Lett.*, vol. 28(12), pp. 1149–1151, Dec. 2018.
- [23] P. Vélez, J. Muñoz-Enano, K. Grenier, J. Mata-Contreras, D. Dubuc, F. Martín, "Split ring resonator (SRR) based microwave fluidic sensor for electrolyte concentration measurements", *IEEE Sensors J.*, vol. 19, no. 7, pp. 2562–2569, Apr. 2019.
- [24] P. Vélez, J. Muñoz-Enano, M. Gil, J. Mata-Contreras, and F. Martín, "Differential microfluidic sensors based on dumbbell-shaped defect ground structures in microstrip technology: analysis, optimization, and applications", *Sensors*, vol. 19, page 3189, 2019.
- [25] J. Muñoz-Enano, P. Vélez, M. Gil, F. Martín, "An analytical method to implement high sensitivity transmission line differential sensors for dielectric constant measurements", *IEEE Sensors J.*, vol. 20, pp. 178–184, Jan. 2020.
- [26] P. Vélez, J. Muñoz-Enano and F. Martín, "Differential sensing based on quasi-microstrip-mode to slot-mode conversion", *IEEE Microw. Wireless Compon. Lett.*, vol. 29, pp. 690–692, Oct. 2019.
- [27] M. Gil, P. Vélez, F. Aznar, J. Muñoz-Enano, and F. Martín, "Differential sensor based on electro-inductive wave (EIW) transmission lines for dielectric constant measurements and defect detection", *IEEE Trans. Ant. Propag.*, vol. 68, pp. 1876–1886, Mar. 2020.
- [28] J. Muñoz-Enano, P. Vélez, M. Gil, J. Mata-Contreras, and F. Martín, "Differential-mode to common-mode conversion detector based on rat-race couplers: analysis and application to microwave sensors and comparators", *IEEE Trans. Microw. Theory Techn.*, vol. 68, pp. 1312–1325, Apr. 2020.
- [29] J. Naqui, *Symmetry Properties in Transmission Lines Loaded with Electrically Small Resonators*, Springer, Heidelberg, Germany, 2016.
- [30] J. Naqui, M. Durán-Sindreu and F. Martín, "Novel sensors based on the symmetry properties of split ring resonators (SRRs)," *Sensors*, vol. 11, pp. 7545–7553, 2011.
- [31] J. Naqui, M. Durán-Sindreu, and F. Martín, "Alignment and position sensors based on split ring resonators," *Sensors*, vol. 12, pp. 11790–11797, 2012.
- [32] B.K. Horestani, C. Fumeaux, S.F. Al-Sarawi, and D. Abbott, "Displacement sensor based on diamond-shaped tapered split ring resonator," *IEEE Sens. J.*, vol. 13, pp. 1153–1160, 2013.
- [33] B.K. Horestani, D. Abbott, and C. Fumeaux, "Rotation sensor based on horn-shaped split ring resonator," *IEEE Sens. J.*, vol. 13, pp. 3014–3015, 2013.
- [34] J. Naqui and F. Martín, "Transmission lines loaded with bisymmetric resonators and their application to angular displacement and velocity sensors," *IEEE Trans. Microw. Theory Techn.*, vol. 61, no. 12, pp. 4700–4713, Dec. 2013.
- [35] J. Naqui and F. Martín, "Angular displacement and velocity sensors based on electric-LC (ELC) loaded microstrip lines," *IEEE Sensors J.*, vol. 14, no. 4, pp. 939–940, Apr. 2014.
- [36] B.K. Horestani, J. Naqui, D. Abbott, C. Fumeaux, and F. Martín, "Two-dimensional displacement and alignment sensor based on reflection coefficients of open microstrip lines loaded with split ring resonators," *Elec. Lett.*, vol. 50, pp. 620–622, Apr. 2014.
- [37] B. Ebrahimi, W. Withayachumankul, S. F. Al-Sarawi and D. Abbott, "Metamaterial-Inspired Rotation Sensor With Wide Dynamic Range," *IEEE Sensors J.*, vol. 14, no. 8, pp. 2609–2614, Aug. 2014.
- [38] J. Naqui, J. Coromina, B. Karami-Horestani, C. Fumeaux, and F. Martín, "Angular displacement and velocity sensors based on coplanar waveguides (CPWs) loaded with S-shaped split ring resonator (S-SRR)," *Sensors*, vol. 15, pp. 9628–9650, 2015.
- [39] J. Mata-Contreras, C. Herrojo, and F. Martín, "Application of split ring resonator (SRR) loaded transmission lines to the design of angular displacement and velocity sensors for space applications", *IEEE Trans. Microw. Theory Techn.*, vol. 65, no. 11, pp. 4450–4460, Nov. 2017.
- [40] J. Mata-Contreras, C. Herrojo, and F. Martín, "Detecting the rotation direction in contactless angular velocity sensors implemented with rotors loaded with multiple chains of split ring resonators (SRRs)", *IEEE Sensors J.*, vol.18, no. 17, pp. 7055–7065, Sep. 2018.
- [41] B. Ebrahimi, J. Scott, K. Ghorbani, "Microwave reflective biosensor for glucose level detection in aqueous solutions", *Sens. & Act. A: Physical*, vol. 301, p. 111662, 2020.
- [42] J. Muñoz-Enano, P. Vélez, M. Gil, and F. Martín, "Microfluidic reflective-mode differential sensor based on open split ring resonators (OSRRs)", *Int. J. Microw. Wireless Technol.*, published online, DOI: doi:10.1017/S1759078720000501.
- [43] D.M. Pozar, *Microwave Engineering*, 4<sup>th</sup> Ed., John Wiley, Hoboken, NJ, 2011.
- [44] B. R. H. Alhawari, B. Ismail, M. B. Mahdi, and R. S. B. Raja Abdullah, "Development of novel tunable dual-band negative index metamaterial using open stub-loaded stepped-impedance resonator", *Prog. Electromagn. Res. B*, vol. 35, pp. 111–131, 2011.
- [45] J. Naqui, M. Durán-Sindreu, J. Bonache and F. Martín, "Implementation of shunt connected series resonators through stepped-impedance shunt stubs: analysis and limitations", *IET Microw. Ant. Propag.*, vol. 5, pp. 1336–1342, Aug. 2011.



**Jonathan Muñoz-Enano** (S'19) was born in Mollet del Vallès (Barcelona), Spain, in 1994. He received the Bachelor's Degree in Electronic Telecommunications Engineering in 2016 and the Master's Degree in Telecommunications Engineering in 2018, both at the Autonomous University of Barcelona (UAB). Actually, he is working in the same university in the elaboration of his PhD, which is focused on the development of microwave sensors based on metamaterials concepts for the dielectric characterization of materials and biosensors.



**Paris Vélez** (S'10–M'14) was born in Barcelona, Spain, in 1982. He received the degree in Telecommunications Engineering, specializing in electronics, the Electronics Engineering degree, and the Ph.D. degree in Electrical Engineering from the Universitat Autònoma de Barcelona, Barcelona, in 2008, 2010, and 2014, respectively. His Ph.D. thesis concerned common mode suppression differential microwave circuits based on metamaterial concepts and semi-lumped resonators. During the Ph.D., he was

awarded with a pre-doctoral teaching and research fellowship by the Spanish Government from 2011 to 2014. From 2015-2017, he was involved in the subjects related to metamaterials sensors for fluidics detection and characterization at LAAS-CNRS through a TECNIOSpring fellowship cofounded by the Marie Curie program. His current research interests include the miniaturization of passive circuits RF/microwave and sensors-based metamaterials through Juan de la Cierva fellowship. Dr. Vélez is a Reviewer for the IEEE Transactions on Microwave Theory and Techniques and for other journals.



**Lijuan Su** was born in Qianjiang (Hubei), China in 1983. She received the B.S. degree in communication engineering and the M.S. degree in circuits and systems both from Wuhan University of Technology, Wuhan, China, in 2005 and 2013 respectively, and the Ph.D. degree in electronic engineering from Universitat Autònoma de Barcelona, Barcelona, Spain, in 2017. From Nov. 2017 to Dec. 2019, she worked as a postdoc

researcher in Flexible Electronics Research Center, Huazhong University of Science and Technology, Wuhan, China. She is currently a postdoc researcher in CIMITEC, Universitat Autònoma de Barcelona, Spain. Her current research interests focus on the development of novel microwave sensors with improved performance for biosensors, dielectric characterization of solids and liquids, defect detection, industrial processes, etc.



**Marta Gil Barba** (S'05–M'09) was born in Valdepeñas, Ciudad Real, Spain, in 1981. She received the Physics degree from Universidad de Granada, Spain, in 2005, and the Ph.D. degree in electronic engineering from the Universitat Autònoma de Barcelona, Barcelona, Spain, in 2009. She studied one year with the Friedrich Schiller Universität Jena, Jena, Germany. During her PhD Thesis she was holder of a METAMORPHOSE NoE grant and National Research Fellowship from the

FPU Program of the Education and Science Spanish Ministry. As a postdoctoral researcher, she was awarded with a Juan de la Cierva fellowship working in the Universidad de Castilla-La Mancha. She was postdoctoral researcher in the Institut für Mikrowellentechnik und Photonik in Technische Universität Darmstadt and in the Carlos III University of Madrid. She is currently assistant professor in the Universidad Politécnica de Madrid. She has worked in metamaterials, piezoelectric MEMS and microwave passive devices. Her current interests include metamaterials sensors for fluidic detection.



**Pau Casacuberta** was born in Sabadell (Barcelona), Spain, in 1997. Currently he is in his senior year of the Bachelor's Degree in Electronic Telecommunications Engineering and the Bachelor's Degree in Computer Engineering, both at the Universitat Autònoma de Barcelona (UAB). He received the Collaboration fellowship by the Spanish Government in 2019 and developing his Bachelor's Thesis in highly sensitive microwave

sensors based in stepped impedance structures.



**Ferran Martín** (M'04–SM'08–F'12) was born in Barakaldo (Vizcaya), Spain in 1965. He received the B.S. Degree in Physics from the Universitat Autònoma de Barcelona (UAB) in 1988 and the PhD degree in 1992. From 1994 up to 2006 he was Associate Professor in Electronics at the Departament d'Enginyeria Electrònica (Universitat Autònoma de Barcelona), and since 2007 he is Full Professor of Electronics. In recent years, he has been involved in different research activities including

modelling and simulation of electron devices for high frequency applications, millimeter wave and THz generation systems, and the application of electromagnetic bandgaps to microwave and millimeter wave circuits. He is now very active in the field of metamaterials and their application to the miniaturization and optimization of microwave circuits and antennas. Other topics of interest include microwave sensors and RFID systems, with special emphasis on the development of high data capacity chipless-RFID tags. He is the head of the Microwave Engineering, Metamaterials and Antennas Group (GEMMA Group) at UAB, and director of CIMITEC, a research Center on Metamaterials supported by TECNIO (Generalitat de Catalunya). He has organized several international events related to metamaterials and related topics, including Workshops at the IEEE International Microwave Symposium (years 2005 and 2007) and European Microwave Conference (2009, 2015 and 2017), and the Fifth International Congress on Advanced Electromagnetic Materials in Microwaves and Optics (Metamaterials 2011), where he acted as Chair of the Local Organizing Committee. He has acted as Guest Editor for six Special Issues on metamaterials and sensors in five International Journals. He has authored and co-authored over 600 technical conference, letter, journal papers and book chapters, he is co-author of the book on Metamaterials entitled *Metamaterials with Negative Parameters: Theory, Design and Microwave Applications* (John Wiley & Sons Inc.), author of the book *Artificial Transmission Lines for RF and Microwave Applications* (John Wiley & Sons Inc.), co-editor of the book *Balanced Microwave Filters* (Wiley/IEEE Press) and co-author of the book *Time-Domain Signature Barcodes for Chipless-RFID and Sensing Applications* (Springer). Ferran Martín has generated 21 PhDs, has filed several patents on metamaterials and has headed several Development Contracts.

Prof. Martín is a member of the IEEE Microwave Theory and Techniques Society (IEEE MTT-S). He is reviewer of the IEEE Transactions on Microwave Theory and Techniques and IEEE Microwave and Wireless Components Letters, among many other journals, and he serves as member of the Editorial Board of IET Microwaves, Antennas and Propagation, International Journal of RF and Microwave Computer-Aided Engineering, and Sensors. He is also a member of the Technical Committees of the European Microwave Conference (EuMC) and International Congress on Advanced Electromagnetic Materials in Microwaves and Optics (Metamaterials). Among his distinctions, Ferran Martín has received the 2006 Duran Farell Prize for Technological Research, he holds the *Parc de Recerca UAB – Santander* Technology Transfer Chair, and he has been the recipient of three ICREA ACADEMIA Awards (calls 2008, 2013 and 2018). He is Fellow of the IEEE and Fellow of the IET.